

# A universal framework for $t$ -channel dark matter models

Chiara Arina<sup>a,1</sup>, Benjamin Fuks<sup>b,2,3</sup>, Luca Mantani<sup>c,1</sup>

<sup>1</sup>Centre for Cosmology, Particle Physics and Phenomenology (CP3), Université catholique de Louvain, B-1348 Louvain-la-Neuve, Belgium

<sup>2</sup>Sorbonne Université, CNRS, Laboratoire de Physique Théorique et Hautes Énergies, LPTHE, F-75005 Paris, France

<sup>3</sup>Institut Universitaire de France, 103 boulevard Saint-Michel, 75005 Paris, France

Received: date / Accepted: date

**Abstract** We present the `DMSimpt` model implementation in `FEYNRULES`, which aims to offer a unique general framework allowing for all simulations relevant for simplified  $t$ -channel dark matter models at colliders and for the complementary cosmology calculations. We describe how to match next-to-leading-order QCD fixed-order calculations with parton showers to derive robust bounds and predictions in the context of LHC dark matter searches, and moreover validate two model restrictions (relevant for Dirac and Majorana fermionic dark matter respectively) to exemplify how to evaluate dark matter observables to constrain the model parameter space. More importantly, we emphasise how to achieve these results by using a combination of publicly available automated tools, and discuss how dark matter predictions are sensitive to the model file and software setup. All files, together with illustrative `MATHEMATICA` notebooks, are available from the URL <http://feynrules.irmp.ucl.ac.be/wiki/DMSimpt>.

## 1 Introduction

Despite of convincing evidence for its existence [1], dark matter still evades direct detection both in dedicated underground nuclear recoil experiments and at colliders. Getting insights on the nature of dark matter and the way in which it interacts with the Standard Model particles therefore consists in one of the hot topics in particle and astroparticle physics today. One potential strategy that could shed light on this matter involves simplified models [2, 3] in which the Standard Model is minimally extended in terms of particles and new

couplings. This approach allows for the exploration of viable dark matter scenarios in a model-independent way and the comparison of theoretical predictions with results of direct, indirect and collider searches. This however requires the ability of making predictions for large classes of models, both at colliders and for what concerns cosmology. The `FEYNRULES` package [4] offers such a possibility, as from a unique `FEYNRULES` implementation of any given dark matter model, it is subsequently possible to generate model files suitable for various high-energy physics tools such as `MG5_AMC` [5], `MADDM` [6] or `MICROMEAS` [7]. Following the general strategy for new physics computations outlined in ref. [8], such a joint usage of various packages has two major advantages in the dark matter context. First, it allows for the straightforward and automatic calculation of the dark matter relic density, as well as of the direct and indirect detection cross sections to verify the cosmological viability of any model. Second, it enables the extraction of the exclusion levels of various searches at colliders through the automated generation of realistic collision events and the recasting of the corresponding LHC analyses. In the latter case, the `MG5_AMC` framework allows in particular for simulations including next-to-leading order corrections in  $\alpha_s$ , so that predictions are accurate enough to derive robust constraints when LHC recasting is at stake through, *e.g.*, the `MADANALYSIS 5` platform [9] that includes, from version 1.8, the propagation of the theoretical uncertainties on the signal predictions up to the derived exclusion levels [10].

In most simplified models for dark matter, the dark matter is assumed to be a single massive particle that interacts weakly with the Standard Model through a mediator particle. In  $s$ -channel setups [11, 12], the mediator is colour-singlet and is enforced to couple to a pair of either dark matter particles, or Standard Model

<sup>a</sup>e-mail: chiara.arina@uclouvain.be

<sup>b</sup>e-mail: fuks@lpthe.jussieu.fr

<sup>c</sup>e-mail: luca.mantani@uclouvain.be

particles. Such a configuration generally arises in scenarios in which the dark matter stability is guaranteed by a  $\mathbb{Z}_2$  discrete symmetry under which all Standard Model fields and the mediator are even, and the dark matter particle is odd. A comprehensive approach for achieving automatic and straightforward cosmological calculations and collider simulations for  $s$ -channel dark matter models has been recently proposed [11], the cornerstone being a unique FEYNRULES implementation driving any subsequent computation. The present work is dedicated to a general implementation, in the FEYNRULES package, of many  $t$ -channel dark matter models in which the mediator interacts with one of the Standard Model quarks and dark matter.

We have used this FEYNRULES implementation to generate a UFO library [13] that can subsequently be imported in programmes like MG5\_AMC or MADDM for undertaking various simulations and computations for a large class of  $t$ -channel dark matter models. Our implementation in particular allows for collider simulations systematically including next-to-leading-order (NLO) QCD corrections to all new physics processes involving either the dark matter particle, the mediator or both. Such a possibility requires however a specific treatment of the real emission contributions that feature, in  $t$ -channel dark matter models, narrow  $s$ -channel resonances. Their integration over the phase space leads to a growth proportional to an inverse power of the resonance width, so that such contributions could be numerically dominant and apparently spoil the convergence of the perturbative series. Moreover, when all new physics processes allowed by the model are considered as a whole (as each subprocess contributes to the new physics signal), these resonant diagrams could be double-counted and lead to incorrect predictions. They therefore need to be treated consistently. Different strategies to treat these resonances have been recently automated within the MG5\_AMC framework [14], hence enabling NLO QCD simulations for the considered  $t$ -channel dark matter models in a way that is as easy as for the  $s$ -channel case.

In order to illustrate the strength of our approach, we focus on two limiting cases and study their phenomenology at colliders and in cosmology, which allows for the validation of our implementation. We in particular compare the performances of MADDM and MICROMEGAS and present, for the first time, automated computations for loop-induced processes relevant for dark matter indirect detection. Such a feature, which will be available from the next release of MADDM, greatly eases the phenomenological analysis of  $t$ -channel dark matter models. More specifically, we consider the case of a fermionic dark matter particle whose interac-

tions with the Standard Model are mediated by a scalar particle coupling to the right-handed up quark, both for what concerns Dirac and Majorana dark matter. In the following, we coin these two configurations, that have been vastly studied in the literature (as shown *e.g.* in refs. [15–30]) and that are particularly promising for LHC and dark matter searches (see *e.g.* refs. [31, 32]), the S3D\_uR and S3M\_uR models, respectively.

The rest of the paper is structured as follows. In the next section, we present the model conventions, its implementation into FEYNRULES and the restrictions (*i.e.* the limiting cases) shipped with our general implementation. In section 3, we detail how to match NLO QCD calculations with parton showers for collider simulations, providing extensive details on how to make use of MG5\_AMC in order to ensure a consistent treatment of the resonant contributions appearing at  $\mathcal{O}(\alpha_s)$ . We then present, for the first time, total rate and differential distributions extracted from accurate predictions matching NLO QCD calculations with parton showers, and derive the corresponding constraints from selected LHC searches. In section 4, we briefly outline the dark matter observables relevant for  $t$ -channel dark matter models, how to compute them with MADDM, and present the results for the S3D\_uR and S3M\_uR model restrictions to validate our implementation against known results. We summarise our work in section 5.

## 2 FEYNRULES implementation and conventions

### 2.1 Generalities

We consider a generic  $t$ -channel dark matter simplified model in which the Standard Model (SM) is extended by several incarnations of two extra fields, a dark matter candidate (that we generically denote by  $X$ ) and a mediator lying in the fundamental representation of  $SU(3)_c$  (that we generically denote by  $Y$ ). In order to maintain the model as general as possible, we allow for several options for the spin of the new particles and therefore include six new dark matter fields  $\tilde{S}$ ,  $S$ ,  $\tilde{\chi}$ ,  $\chi$ ,  $\tilde{V}_\mu$  and  $V_\mu$ , all lying in the singlet representation of the SM gauge group  $SU(3)_c \times SU(2)_L \times U(1)_Y$ . These fields respectively correspond to a real scalar field, a complex scalar field, a Majorana spinor, a Dirac spinor, a real vector field and a complex vector field. The most general Lagrangian embedding all the interactions of these fields with the SM can be written, after imposing that electroweak gauge invariance is preserved, as

$$\begin{aligned} \mathcal{L} = & \mathcal{L}_{\text{SM}} + \mathcal{L}_{\text{kin}} + \mathcal{L}_F(\chi) + \mathcal{L}_F(\tilde{\chi}) \\ & + \mathcal{L}_S(S) + \mathcal{L}_S(\tilde{S}) + \mathcal{L}_V(V) + \mathcal{L}_V(\tilde{V}), \end{aligned} \quad (1)$$

Field	Spin	Repr.	Self-conj.	FEYNRULES name	PDG
$\tilde{S}$	0	$(\mathbf{1}, \mathbf{1}, 0)$	yes	Xs	51
$S$	0	$(\mathbf{1}, \mathbf{1}, 0)$	no	Xc	56
$\tilde{\chi}$	1/2	$(\mathbf{1}, \mathbf{1}, 0)$	yes	Xm	52
$\chi$	1/2	$(\mathbf{1}, \mathbf{1}, 0)$	no	Xd	57
$\tilde{V}_\mu$	1	$(\mathbf{1}, \mathbf{1}, 0)$	yes	Xv	53
$V_\mu$	1	$(\mathbf{1}, \mathbf{1}, 0)$	no	Xw	58
$\varphi_Q = \begin{pmatrix} \varphi_Q^{(u)} \\ \varphi_Q^{(d)} \end{pmatrix}$	0	$(\mathbf{3}, \mathbf{2}, \frac{1}{6})$	no	YS3Q = $\begin{pmatrix} \text{YS3Qu} \\ \text{YS3Qd} \end{pmatrix}$	$\varphi_Q^{(u)}$ : 1000002 1000004 1000006 $\varphi_Q^{(d)}$ : 1000001 1000003 1000005
$\varphi_u$	0	$(\mathbf{3}, \mathbf{1}, \frac{2}{3})$	no	YS3u	2000002 2000004 2000006
$\varphi_d$	0	$(\mathbf{3}, \mathbf{1}, -\frac{1}{3})$	no	YS3d	2000001 2000003 2000005
$\psi_Q = \begin{pmatrix} \psi_Q^{(u)} \\ \psi_Q^{(d)} \end{pmatrix}$	1/2	$(\mathbf{3}, \mathbf{2}, \frac{1}{6})$	no	YF3Q = $\begin{pmatrix} \text{YF3Qu} \\ \text{YF3Qd} \end{pmatrix}$	$\psi_Q^{(u)}$ : 5910002 5910004 5910006 $\psi_Q^{(d)}$ : 5910001 5910003 5910005
$\psi_u$	1/2	$(\mathbf{3}, \mathbf{1}, \frac{2}{3})$	no	YF3u	5920002 5920004 5920006
$\psi_d$	1/2	$(\mathbf{3}, \mathbf{1}, -\frac{1}{3})$	no	YF3d	5920001 5920003 5920005

**Table 1** New particles supplementing the Standard Model field content, given together with their representations under  $SU(3)_c \times SU(2)_L \times U(1)_Y$ , their Majorana nature, their name in the FEYNRULES implementation and the associated Particle Data Group (PDG) identifiers. Three generations of mediators (second part of the table) are included.

where  $\mathcal{L}_{\text{SM}}$  is the SM Lagrangian and  $\mathcal{L}_{\text{kin}}$  contains gauge-invariant kinetic and mass terms for all new fields. The fermionic, scalar and vector dark matter Lagrangians read

$$\begin{aligned}
\mathcal{L}_F(X) &= \left[ \lambda_Q \bar{X} Q \varphi_Q^\dagger + \lambda_u \bar{X} u \varphi_u^\dagger + \lambda_d \bar{X} d \varphi_d^\dagger + \text{h.c.} \right], \\
\mathcal{L}_S(X) &= \left[ \hat{\lambda}_Q \bar{\psi}_Q Q X + \hat{\lambda}_u \bar{\psi}_u u X + \hat{\lambda}_d \bar{\psi}_d d X + \text{h.c.} \right], \quad (2) \\
\mathcal{L}_V(X) &= \left[ \hat{\lambda}_Q \bar{\psi}_Q \not{X} Q + \hat{\lambda}_u \bar{\psi}_u \not{X} u + \hat{\lambda}_d \bar{\psi}_d \not{X} d + \text{h.c.} \right].
\end{aligned}$$

In our notation,  $Q$  stands for the  $SU(2)_L$  doublet of left-handed quarks and  $u$  and  $d$  are the up-type and down-type  $SU(2)_L$  singlets of right-handed quarks respectively. The scalar mediators  $\varphi_Q$ ,  $\varphi_u$  and  $\varphi_d$  are chosen to solely interact with the  $Q$ ,  $u$  and  $d$  quarks, as for the fermionic mediators  $\psi_Q$ ,  $\psi_u$  and  $\psi_d$  (that are thus vector-like). The mediators therefore lie in the same SM representation as their quark partners. In the above expression, we have understood all flavour indices for clarity. The  $\lambda_Q$ ,  $\lambda_u$  and  $\lambda_d$  coupling strengths are hence  $3 \times 3$  matrices in the flavour space, that we moreover consider real and flavour-diagonal for simplicity.

The new physics particles of the simplified model are given in table 1, together with their representation under the gauge and Poincaré groups, their potential Majorana nature, the adopted particle name in the FEYNRULES implementation and the adopted Particle Data Group (PDG) identifiers [33]. The conventions for the different coupling parameters are summarised in table 2, in which they are given together with the name used in the FEYNRULES implementation and the Les

Coupling	FEYNRULES name	LH block
$(\lambda_Q)_{ij}$	1amS3Q	DMS3Q
$(\lambda_u)_{ij}$	1amS3u	DMS3U
$(\lambda_d)_{ij}$	1amSdD	DMS3D
$(\hat{\lambda}_Q)_{ij}$	1amF3Q	DMF3Q
$(\hat{\lambda}_u)_{ij}$	1amF3u	DMF3U
$(\hat{\lambda}_d)_{ij}$	1amF3d	DMF3D

**Table 2** New couplings dictating the interactions of the new particles with the Standard Model sector. Each coupling is given together with the associated FEYNRULES symbol and the Les Houches (LH) block of the parameter card.

Houches (LH) blocks [34] storing their numerical values when running tools like MG5-AMC or MADDM.

By relying on a joint usage of the FEYNRULES [4], NLOCT [35] and FEYNARTS [36] packages, we automatically generate a UFO model [13] that can be used by MG5-AMC for both leading order (LO) and NLO computations. This UFO model includes all UV counterterms allowing for the renormalisation of the model with respect to the QCD interactions, as well as all  $R_2$  Feynman rules that are relevant for the numerical evaluation of one-loop integrals in four dimensions.

The model is shipped with a large ensemble of restrictions dedicated to specific  $t$ -channel simplified models. These are summarised in table 3 where for each restriction, we specify the active new physics states, all other states being taken decoupled and non-interacting. In other words, each restriction consists in a simplified

Name	DM	Mediators	Parameters
S3M_uni	$\tilde{\chi}$	$\varphi_{Q_f}, \varphi_{u_f}, \varphi_{d_f}$	$M_\varphi, M_\chi, \lambda_\varphi$
S3D_uni	$\chi$		
S3M_3rd	$\tilde{\chi}$		
S3D_3rd	$\chi$	$\varphi_{Q_3}, \varphi_{u_3}, \varphi_{d_3}$	
S3M_uR	$\tilde{\chi}$		
S3D_uR	$\chi$		
F3S_uni	$\tilde{S}$	$\psi_{Q_f}, \psi_{u_f}, \psi_{d_f}$	$M_S, M_\psi, \hat{\lambda}_\psi$
F3C_uni	$S$		
F3S_3rd	$\tilde{S}$		
F3C_3rd	$S$	$\psi_{Q_3}, \psi_{u_3}, \psi_{d_3}$	
F3S_uR	$\tilde{S}$		
F3C_uR	$S$		
F3V_uni	$\tilde{V}_\mu$	$\psi_{Q_f}, \psi_{u_f}, \psi_{d_f}$	$M_V, M_\psi, \hat{\lambda}_\psi$
F3W_uni	$V_\mu$		
F3V_3rd	$\tilde{V}_\mu$		
F3W_3rd	$V_\mu$	$\psi_{Q_3}, \psi_{u_3}, \psi_{d_3}$	
F3V_uR	$\tilde{V}_\mu$		
F3W_uR	$V_\mu$		
		$\varphi_{u_1}$	
		$\psi_{u_1}$	

**Table 3** List of all restrictions included in the DMSimpT UFO model. In each case, the simplified model contains a single class of mass-degenerate mediators (where  $f = 1, 2, 3$  is a flavour index), a specific dark matter candidate and universal and flavour-conserving dark matter couplings  $\lambda_\varphi$  and  $\hat{\lambda}_\psi$ .

model in which the SM is extended by a specific class of mediators, and a given dark matter state. In order to reduce the number of free parameters, all (active) mediators are taken mass-degenerate. A given restriction named XYZ can be loaded in MG5\_AMC (or MADDM) by typing, within the tool command line interface,

```
import model DMSimp_t-XYZ --modelname
```

In the model restrictions whose name ends with the **uni** suffix, all twelve flavours of mediators are considered, their mass and interaction strengths being taken flavour-conserving and universal,

$$(\lambda_F)_{ij} = \lambda_\varphi \delta_{ij} \quad \text{and} \quad (\hat{\lambda}_F)_{ij} = \hat{\lambda}_\psi \delta_{ij}, \quad (3)$$

for  $F = Q, u$  and  $d$ . In model restrictions of the **uR** class, only mediators coupling to the right-handed up quark are taken as active,

$$(\lambda_u)_{11} = \lambda_\varphi \quad \text{and} \quad (\hat{\lambda}_u)_{11} = \hat{\lambda}_\psi, \quad (4)$$

all other couplings being vanishing, whilst in the **3rd** class of model restrictions, we only consider the mediator coupling to the third generation of SM quarks,

$$(\lambda_Q)_{33} = (\lambda_u)_{33} = (\lambda_d)_{33} = \lambda_\varphi, \quad (5)$$

$$(\hat{\lambda}_Q)_{11} = (\hat{\lambda}_u)_{22} = (\hat{\lambda}_d)_{33} = \hat{\lambda}_\psi,$$

all other couplings being again assumed vanishing.

## 2.2 The S3M/S3D class of models

In **S3M**-type and **S3D**-type models, the dark matter is taken to be respectively the Majorana and Dirac state  $\tilde{\chi}$  and  $\chi$  of mass  $M_\chi$ . As written in section 2.1, all mediators are considered degenerate of mass  $M_\varphi$ , and all new physics interactions are universal and flavour-conserving with a global strength  $\lambda_\varphi$ . The generic Lagrangian  $\mathcal{L}_F$  of eq. (2) therefore simplifies to

$$\mathcal{L}_{X\_uni}(X) = \sum_{F=Q,u,d} \sum_{f=1}^3 \left[ \lambda_\varphi \bar{X} F_f \varphi_{Ff}^\dagger + \text{h.c.} \right], \quad (6)$$

where  $X = \chi$  (**S3D**) or  $\tilde{\chi}$  (**S3M**) equivalently refers to Dirac or Majorana dark matter, and  $f$  is a generation index. The model is thus defined by three parameters,

$$\{M_\chi, M_\varphi, \lambda_\varphi\}. \quad (7)$$

In the universal **S3M\_uni** and **S3D\_uni** restrictions, the simplified model includes all twelve mediators, whilst in the **S3M\_3rd** and **S3D\_3rd** restrictions, the setup is further simplified and dark matter only couples to the third generation via the four corresponding mediators. In the **S3M\_uR** and **S3D\_uR** restrictions, only a coupling to the right-handed up quark  $u_1$  is considered, through a single mediator. The associated Lagrangians read,

$$\mathcal{L}_{X\_3rd}(X) = \sum_{F=Q,u,d} \left[ \lambda_\varphi \bar{X} F_3 \varphi_{F3}^\dagger + \text{h.c.} \right], \quad (8)$$

$$\mathcal{L}_{X\_uR}(X) = \left[ \lambda_\varphi \bar{X} u_1 \varphi_{u1}^\dagger + \text{h.c.} \right].$$

## 2.3 The F3S/F3C class of models

In **F3S**-type and **F3C**-type models, the dark matter consists of the real and complex scalar state  $\tilde{S}$  and  $S$  of mass  $M_S$  respectively. As in the previous subsection, all mediators are assumed to be degenerate of mass  $M_\psi$ , and all new physics interactions are universal and flavour-conserving with a strength  $\hat{\lambda}_\psi$ . The Lagrangian  $\mathcal{L}_S$  of eq. (2) therefore simplifies to

$$\mathcal{L}_{X\_uni}(X) = \sum_{F=Q,u,d} \sum_{f=1}^3 \left[ \hat{\lambda}_\psi \bar{\psi}_{Ff} F_f X + \text{h.c.} \right], \quad (9)$$

where  $X = \tilde{S}$  (**F3S**) and  $S$  (**F3C**) in the real and complex case. The model is defined by three parameters,

$$\{M_S, M_\psi, \hat{\lambda}_\psi\}. \quad (10)$$

In the universal **F3S\_uni** and **F3C\_uni** restrictions, dark matter couples to all SM quark eigenstates through twelve mediators. In the third generation **F3S\_3rd** and

**F3C\_3rd** models, its couplings are restricted to the bottom and top quark ones and the corresponding four mediators, while in the **F3S\_uR** and **F3C\_uR** models, dark matter only couples to the right-handed up quark. The associated Lagrangians are

$$\begin{aligned}\mathcal{L}_{\text{X}_3\text{rd}}(X) &= \sum_{F=Q,u,d} \left[ \hat{\lambda}_\psi \bar{\psi}_{F_3} F_3 X + \text{h.c.} \right], \\ \mathcal{L}_{\text{X}_u\text{R}}(X) &= \left[ \hat{\lambda}_\psi \bar{\psi}_{u_1} u_1 X + \text{h.c.} \right].\end{aligned}\quad (11)$$

## 2.4 The F3V/F3W class of models

In the **F3V** and **F3W** types of models, the dark matter is a real and complex vector state  $\tilde{V}_\mu$  and  $V_\mu$  of mass  $M_V$  respectively. All mediators are degenerate of mass  $M_\psi$ , and all new physics interactions are universal and flavour-conserving with a common strength  $\hat{\lambda}_\psi$ . The Lagrangian  $\mathcal{L}_V$  of eq. (2) is simplified to

$$\mathcal{L}_{\text{X}_\text{uni}}(X) = \sum_{F=Q,u,d} \sum_{f=1}^3 \left[ \hat{\lambda}_\psi \bar{\psi}_{F_f} \not{X} F_f + \text{h.c.} \right], \quad (12)$$

where  $X = \tilde{V}$  (**F3V**) or  $V$  (**F3W**) in the real and complex vector case. The model is defined by three parameters,

$$\{M_V, M_\psi, \hat{\lambda}_\psi\}. \quad (13)$$

In the **F3V\_uni** and **F3W\_uni** restrictions, all twelve mediators are included. In contrast, in the **F3V\_3rd** and **F3W\_3rd** restrictions, only the four mediators relating dark matter to the top and bottom quarks are included, whilst in the **F3V\_uR** and **F3W\_uR** models, the only non-vanishing coupling is the one to the right-handed up-quark. The associated Lagrangians read

$$\begin{aligned}\mathcal{L}_{\text{X}_3\text{rd}}(X) &= \sum_{F=Q,u,d} \left[ \hat{\lambda}_\psi \bar{\psi}_{F_3} \not{X} F_3 + \text{h.c.} \right], \\ \mathcal{L}_{\text{F3S}_u\text{R}}(X) &= \left[ \hat{\lambda}_\psi \bar{\psi}_{u_1} \not{X} u_1 + \text{h.c.} \right].\end{aligned}\quad (14)$$

## 3 Matching NLO QCD fixed-order calculations with parton showers

### 3.1 Generalities

In the class of simplified models under consideration, the computation of NLO QCD corrections involve real emission diagrams possibly featuring intermediate  $s$ -channel resonances. These should be treated consistently in order not to apparently spoil the convergence of the perturbative series by yielding NLO cross sections much larger than the associated LO ones. This occurs when the cross section related to the production of the

resonant state is much larger than the one of the initially considered process. Moreover, we aim at combining events describing all possible new physics processes of a given model at the NLO accuracy in QCD. We will hence consider the production of a pair of dark matter particles ( $pp \rightarrow XX$ ), of any mediators ( $pp \rightarrow Y_i Y_j$ ), as well as the associated production of a mediator and a dark matter state ( $pp \rightarrow XY_i$ ). Therefore, the subtraction of all resonant contributions in the real corrections is mandatory to avoid their double-counting when combining the three types of processes.

Different strategies dealing with the treatment of these resonances have been recently automated within the MG5\_AMC framework [14]. They include diagram removal methods with or without keeping the interferences between the resonant and non-resonant contributions [37], as well as various techniques to subtract the resonant contribution from the full amplitude [38]. In the following, we employ one of such strategies, in which all squared resonant diagram contributions are discarded whilst the interferences of the resonant and non-resonant diagrams are kept. All available methods should however lead to numerically similar results if the resonant process can be consistently defined. In practice, MG5\_AMC has to be run together with the MADSTR plugin<sup>1</sup> that can be activated by starting MG5\_AMC as

```
mg5_amc --mode=MadSTR
```

The code is then used to simulate events, at the NLO accuracy in QCD, relevant for all new physics processes allowed by  $t$ -channel dark matter models. The considered processes can be classified into three categories,

$$\begin{aligned}pp &\rightarrow XX, \\ pp &\rightarrow XY \text{ with } Y \rightarrow Xj, \\ pp &\rightarrow YY \text{ with } Y \rightarrow Xj.\end{aligned}\quad (15)$$

This corresponds to the production of a pair of dark matter particles (generically denoted by  $XX$ ), the associated production of a mediator and a dark matter particle (generically denoted by  $XY$ ), and the production of a pair of mediators (generically denoted by  $YY$ ). In the latter two cases, the mediator further decays into a SM quark and dark matter.

After simulating each process separately, the different contributions are combined, which is only possible if all resonant pieces from the real emission to the three subprocesses are subtracted. For instance, the diagrams associated with the second Born subprocess ( $pp \rightarrow XY \rightarrow XXj$ ) are included in those related to

<sup>1</sup>The MADSTR plugin can be downloaded from <https://code.launchpad.net/~maddevelopers/mg5amcnlo/MadSTRPlugin>



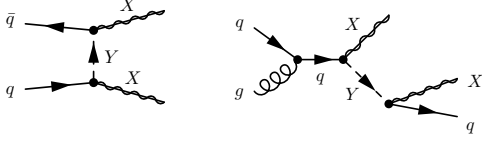


**Fig. 1** Representative LO Feynman diagrams describing the production of a pair of dark matter particles (left) and the associated production of a mediator with a dark matter state (right). The mediator decay into dark matter and a quark is included.

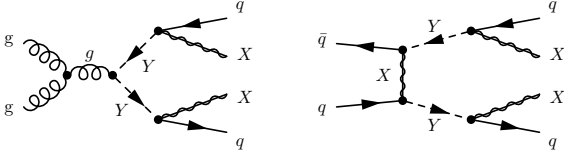


**Fig. 2** Same as figure 1 but for mediator pair-production (and decay) in the QCD (left) and  $t$ -channel dark matter exchange (right) channels.

the real corrections to the first subprocess ( $pp \rightarrow XX$ ). In order to avoid any double counting, we include the resonant component into the Born contribution to  $XY$  production, and the non-resonant one into the real corrections to  $XX$  production.

We import the `DMSimpt` UFO model in `MG5_AMC` to deal with the generation of hard-scattering events at the NLO accuracy for all the processes of eq. (15), using the `MADSTR` plugin and convoluting the matrix elements with the NLO set of NNPDF 3.0 parton distribution functions (PDFs) [39] accessed via the LHAPDF 6 library [40]. Mediator decays are handled with the `MADSPIN` [41] and `MADWIDTH` [42] programmes, which allows for the factorisation of the production and decay processes in a way retaining both off-shell and spin correlation effects. The resulting partonic events are matched with parton showers as described by the `PYTHIA 8` package [43], following the `MC@NLO` prescription [44]. We also use `PYTHIA 8` to handle hadronisation. We then reconstruct the hadron-level events by clustering hadrons according to the anti- $k_T$  algorithm with a separation parameter set to  $\Delta R = 0.4$  [45], as implemented in the `FASTJET` software [46] that we drive from `MADANALYSIS 5` [9, 47]. The latter programme is also used for the generation of the differential distributions studied in section 3.3, and the reinterpretation analysis of the LHC results in section 3.4.

### 3.2 Simulating an `S3D_uR` dark matter signal

In the following, we illustrate how NLO predictions matched with parton showers can be achieved in the

`S3D_uR` class of model. In the  $X/Y$  notations of eq. (15), we thus have,  $X = \chi, \bar{\chi}$  and  $Y = \varphi_{u_1}, \varphi_{u_1}^\dagger$ .

Events originating from dark matter pair production at NLO ( $pp \rightarrow XX$ ; see *e.g.* the left panel of figure 1 for a representative LO Feynman diagram) are generated by starting `MG5_AMC` with the `MADSTR` plugin switched on. The usual `generate` and `output` commands available from the `MG5_AMC` command line interface [5] are then cast, after having imported the restricted UFO model,

```
import model DMSimpt-S3D_uR --modelname
generate p p > xd xd~ / yf3qu1 yf3qu2 \
yf3qu3 yf3qd1 yf3qd2 yf3qd3 yf3u1 yf3u2 \
yf3u3 yf3d1 yf3d2 yf3d3 ys3qu1 ys3qu2 \
ys3qu3 ys3qd1 ys3qd2 ys3qd3 ys3u2 ys3u3 \
ys3d1 ys3d2 ys3d3 xs xm xv [QCD]
output
```

In order for the restricted model to be dealt with consistently, it is crucial to explicitly forbid any decoupled particle to run into any virtual loop. This is implemented at the level of the `generate` command, in which we manually exclude all fermionic mediators, all scalar mediators not coupling to the right-handed up quark  $u_R$  and all irrelevant dark matter states of the model. The UFO conventions for the particle names follow the `FEYNRULES` ones introduced in table 1 (we recall that the `MG5_AMC` command line interface is case insensitive), additionally including an integer number for the generation indices. On run time, the `MADSTR` plugin takes care of identifying and treating any potentially resonant contribution. In our case, the squared resonant contributions are discarded, whilst the interferences of the resonance with the non-resonant continuum are kept.

Events describing the associated production of a mediator with a dark matter particle ( $pp \rightarrow XY$ ; see *e.g.* the right panel of figure 1 for a representative diagram including the mediator decay process) are generated in a similar fashion,

```
import model DMSimpt-S3D_uR --modelname
define dm = xd xd~
define yy1 = ys3u1 ys3u1~
generate p p > dm yy1 / yf3qu1 yf3qu2 \
yf3qu3 yf3qd1 yf3qd2 yf3qd3 yf3u1 yf3u2 \
yf3u3 yf3d1 yf3d2 yf3d3 ys3qu1 ys3qu2 \
ys3qu3 ys3qd1 ys3qd2 ys3qd3 ys3u2 ys3u3 \
ys3d1 ys3d2 ys3d3 xs xm xv [QCD]
output
```

where we make use of the `dm` and `yy1` multiparticle labels to guarantee that all potential particle/antiparticle combinations are accounted for.

Mediator pair production is generally dominated by QCD contributions that are independent of the dark matter mass and couplings, as illustrated by the first Feynman diagram of figure 2 that also includes the mediator decay process. However, if  $\lambda_\varphi$  is large enough,  $t$ -channel dark matter exchanges, as depicted by the second diagram of figure 2, could significantly contribute. NLO QCD corrections to the strong contributions to mediator pair-production of  $\mathcal{O}(\alpha_s)$  can be straightforwardly calculated by typing in the MG5\_AMC command line interface,

```
import model DMSimpT-S3D_uR --modelname
define yy1 = ys3u1 ys3u1~
generate p p > yy1 yy1 / yf3qu1 yf3qu2 \
  yf3qu3 yf3qd1 yf3qd2 yf3qd3 yf3u1 yf3u2 \
  yf3u3 yf3d1 yf3d2 yf3d3 ys3qu1 ys3qu2 \
  ys3qu3 ys3qd1 ys3qd2 ys3qd3 ys3u2 ys3u3 \
  ys3d1 ys3d2 ys3d3 xs xm xv [QCD]
output
```

without using the MADSTR plugin. Making use of the coupling order information of the model, MG5\_AMC automatically restricts the process to its pure QCD contribution, neglecting any  $t$ -channel dark matter exchange at the Born level and any real emission or virtual contribution depending on  $\lambda_\varphi$ . The considered Born contribution is thus of  $\mathcal{O}(\alpha_s^2)$  whilst the NLO component is of  $\mathcal{O}(\alpha_s^3)$  and free of any resonance.

The pure  $t$ -channel contribution can be evaluated, at the NLO accuracy in QCD, by typing

```
import model DMSimpT-S3D_uR --modelname
define yy1 = ys3u1 ys3u1~
generate p p > yy1 yy1 DMT=2 QCD=0 QED=0 \
  yf3qu1 yf3qu2 yf3qu3 yf3qd1 yf3qd2 yf3qd3 \
  yf3u1 yf3u2 yf3u3 yf3d1 yf3d2 yf3d3 \
  ys3qu1 ys3qu2 ys3qu3 ys3qd1 ys3qd2 ys3qd3 \
  ys3u2 ys3u3 ys3d1 ys3d2 ys3d3 xs xm xv \
  [QCD]
output
```

The coupling order restriction `DMT=2 QCD=0 QED=0` attached to the `generate` command guarantees that the Born amplitude is proportional to  $\lambda_\varphi^2$  and does not include any contribution depending on  $\alpha_s$  or on the electroweak coupling  $\alpha$ . In other words, any tree-level diagram including a gluon, a photon or a  $Z$ -boson propagator is discarded, so that the Born matrix element is of  $\mathcal{O}(\lambda_\varphi^4)$  and the NLO corrections of  $\mathcal{O}(\lambda_\varphi^4 \alpha_s)$ . In order to deal with the resonant contributions potentially arising at NLO, the MADSTR plugin is used.

Care must be taken when dealing with the mixed-order interferences of the QCD diagrams with the  $t$ -channel ones. The version 3.x.y of MG5\_AMC being incompatible with MADSTR and the version 2.6.x of

the code being unable to handle mixed orders, there is not any publicly available and user-friendly option. One possible way to cure this issue would be to include in the UFO model all UV counterterms and  $R_2$  rational terms necessary for mixed-order NLO calculations in QCD, QED and in the new physics  $\lambda$  coupling, and to implement in MADFKS [48] all necessary subtraction terms. This however goes beyond the scope of this work. We therefore adopt the strategy of simulating the interferences at LO, and reweight the events by a  $K$ -factor assumed to approximate the effect of the QCD corrections. We multiply the interference event weights by the geometric mean of the pure QCD and pure  $t$ -channel  $K$ -factors, those two NLO to LO ratios being defined differentially. In other words, each distribution will be reweighted bin by bin. Event simulation for the interferences is then performed by typing, in the MG5\_AMC command line interface,

```
import model DMSimpT-S3D_uR --modelname
define yy1 = ys3u1 ys3u1~
generate p p > yy1 yy1 DMT^2=2 / yf3qu1 \
  yf3qu2 yf3qu3 yf3qd1 yf3qd2 yf3qd3 yf3u1 \
  yf3u2 yf3u3 yf3d1 yf3d2 yf3d3 ys3qu1 \
  ys3qu2 ys3qu3 ys3qd1 ys3qd2 ys3qd3 ys3u2 \
  ys3u3 ys3d1 ys3d2 ys3d3 xs xm xv
output
```

### 3.3 Total and differential cross sections for S3D\_uR dark matter

In order to illustrate how all subprocesses of eq. (15) could impact a dark matter signal at the LHC, we consider two benchmark scenarios representative of the S3D\_uR model. We fix the dark matter and mediator masses to

$$\begin{aligned} \mathbf{S1.} \quad & M_\chi = 150 \text{ GeV}, \quad M_\varphi = 500 \text{ GeV}, \\ \mathbf{S2.} \quad & M_\chi = 150 \text{ GeV}, \quad M_\varphi = 1000 \text{ GeV}, \end{aligned} \quad (16)$$

and the new physics coupling to

$$\lambda_\varphi = 1. \quad (17)$$

In the first scenario **S1**, the spectrum is more compressed although there is enough phase space for the light mediator to decay into a dark matter particle and a hard jet. In the second scenario **S2**, the mediator is heavier, its mass being fixed to a more realistic value with respect to current squark mass limits [49,50]. Whilst present supersymmetry bounds on the strongly-interacting superpartners are usually stricter, they are not directly applicable to our setup by virtue of the

Scen.	$XX$ [fb]	$XY$ [fb]	$YY$ (total) [fb]	$YY$ (QCD) [fb]	$YY$ ( $t$ -channel) [fb]
<b>S1</b>	$775.3^{+0.4\%}_{-0.8\%} \pm 1.9\%$	$1617^{+16.5\%}_{-13.4\%} \pm 1.0\%$	$473.5^{+23.6\%}_{-16.9\%} \pm 3.0\%$	$324.2^{+34.2\%}_{-23.8\%} \pm 3.4\%$	$261.5^{+7.1\%}_{-6.3\%} \pm 2.5\%$
<b>S2</b>	$122.0^{+1.8\%}_{-2.0\%} \pm 1.9\%$	$74.1^{+20.3\%}_{-15.8\%} \pm 1.2\%$	$7.452^{+19.8\%}_{-14.5\%} \pm 5.6\%$	$3.545^{+37.3\%}_{-25.4\%} \pm 7.2\%$	$6.939^{+11.1\%}_{-9.4\%} \pm 5.0\%$
<b>S1</b>	$929.8^{+1.9\%}_{-1.3\%} \pm 1.9\%$	$2212^{+5.9\%}_{-6.3\%} \pm 1.0\%$	$648.4^{+8.0\%}_{-9.2\%} \pm 3.1\%$	$484.7^{+10.7\%}_{-12.4\%} \pm 3.4\%$	$314.1^{+2.6\%}_{-2.6\%} \pm 2.5\%$
<b>S2</b>	$139.1^{+1.3\%}_{-1.1\%} \pm 2.0\%$	$101.8^{+6.0\%}_{-7.1\%} \pm 1.2\%$	$9.888^{+6.5\%}_{-7.6\%} \pm 5.8\%$	$5.303^{+11.2\%}_{-13.3\%} \pm 7.4\%$	$8.749^{+3.6\%}_{-3.9\%} \pm 4.9\%$

**Table 4** Total cross sections at LO (upper) and NLO (lower), in fb, for the subprocesses of eq. (15) and the benchmark scenarios defined in eqs. (16) and (17). Our predictions are given together with the scale and parton density uncertainties.

different nature of the dark matter and mediator particles. We therefore ignore them for now and address this point in section 3.4.

In table 4, we present total cross sections for the various processes of eq. (15) and for the two considered benchmarks, both at LO (upper panel) and NLO (lower panel) accuracy, and for a setup in which the  $pp \rightarrow XX$  process simulation includes a transverse momentum ( $p_T$ ) cut of 100 GeV on the leading jet at the matrix-element-generator level. For each of the subprocesses, the NLO  $K$ -factor defined as the ratio of the NLO predictions to the LO one is large. This emphasises the relevance of using rates that are NLO-accurate to avoid underestimating signal yields. Our LO and NLO predictions also include theoretical scale uncertainties originating from missing higher-order corrections and those associated with the parton density fit. We estimate the former by a nine-point independent scale variation in which the renormalisation and factorisation scales are varied by a factor of 2 up and down with respect to a central scale set to the average transverse mass of the final-state particles. Except for dark-matter pair-production ( $pp \rightarrow XX$ ) that is insensitive to  $\alpha_s$  at the lowest order (see *e.g.* the left panel of figure 1), LO predictions are affected by large scale uncertainties that are significantly reduced when NLO corrections are included. This consists in the second major benefit of higher-order calculations: the reduction of the theoretical systematics. The second source of theoretical uncertainties, the PDF errors, yields a similar effect at LO and NLO as the same parton density set has been used. Those errors are reasonably small as our benchmark scenarios feature masses leading to a moderate Bjorken- $x$  regime. Additionally, we have verified that the QCD contribution to mediator pair production agrees with the expectation for squark pair-production in a supersymmetric simplified scenario in which all superpartners but a single squark are decoupled [14].

In the right panel of the table, we investigate the impact of the QCD and  $t$ -channel contributions to the production of a pair of mediators. The adopted scenarios, with their large coupling choice of eq. (17), ensure

that the  $t$ -channel contribution is relevant and cannot be neglected. On the contrary, for slightly smaller coupling choices, only QCD production would remain, as the  $t$ -channel amplitude squared is proportional to  $\lambda_\varphi^4$  and the interference between the QCD and  $t$ -channel mode to  $\lambda_\varphi^2$ . For  $\lambda_\varphi = 1$ , the relative importance of the QCD and  $t$ -channel modes turns out to differ for the two benchmark points under consideration. In the case of the **S1** setup, QCD contributions dominate, as expected for such a small mediator mass  $M_\varphi = 500$  GeV. In contrast, for scenarios like the **S2** scenario in which the mediator is much heavier, the QCD production mode is suppressed by virtue of the steeply falling production rate with  $M_\varphi$ , so that the  $t$ -channel contribution dominates. For both cases, the two contributions are however of a similar order of magnitude and their destructive interferences are large. As the two channels are sensitive to different initial partonic luminosities (QCD production being mostly induced by gluon fusion and  $t$ -channel production by quark-antiquark scattering), they feature different PDF uncertainties as well as a different dependence on the unphysical scales.

In figures 3 and 4, we present a few properties of the new physics signal induced by the benchmark scenarios **S1** and **S2** respectively. We focus on observables that are relevant for dark matter searches at the LHC in the monojet channel and consider the description of the missing transverse energy and jet activity. We show differential distributions for the transverse momentum of the leading jet  $p_T(j_1)$  (left panel), the missing transverse energy  $E_T^{\text{miss}}$  (central panel) and the total hadronic activity  $H_T$  (right panel) defined as the scalar sum of the  $p_T$  of all reconstructed jets. For each observable, we present predictions at LO (dashed lines) and NLO (solid lines) for the individual contributions of the processes shown in eq. (15), as well as for their sum (red). We hence distinguish the QCD-induced (teal) and  $t$ -channel-mediated components (blue) of the mediator pair-production channel ( $YY$ ), the dark-matter pair production mode ( $XX$ , purple) and the associated production of a mediator with dark matter ( $XY$ , green). The shaded areas around the NLO results cor-



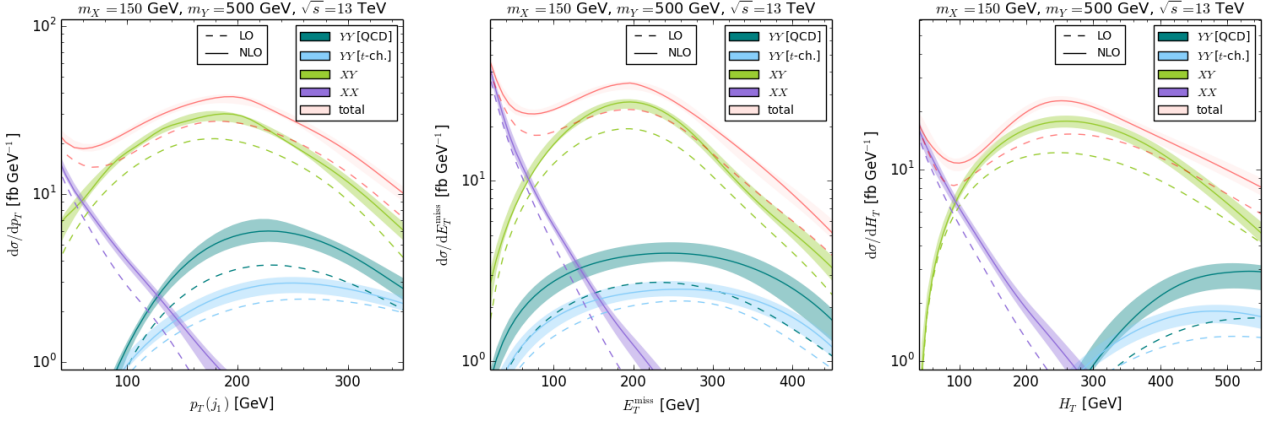


**Fig. 3** Selected properties of the new physics signal emerging from the **S1** scenario. We present the  $p_T$  spectrum of the leading jet (left), as well as the  $E_T^{\text{miss}}$  (central) and  $H_T$  (right) distributions. We consider the separate contributions of the production of a pair of dark matter particles ( $XX$ ; purple), the associated production of a dark matter particle and a mediator ( $XY$ ; green), the QCD-induced production of a pair of mediators ( $YY$  [QCD]; teal) and the  $t$ -channel-induced production of a pair of mediators ( $YY$  [t-ch.]; blue). The sum of all contributions (red) additionally includes the interferences between the two mediator pair-production modes. For all channels, we compare NLO predictions (solid lines) with LO predictions (dashed lines), and represent the NLO scale uncertainty variation bands by shaded areas.

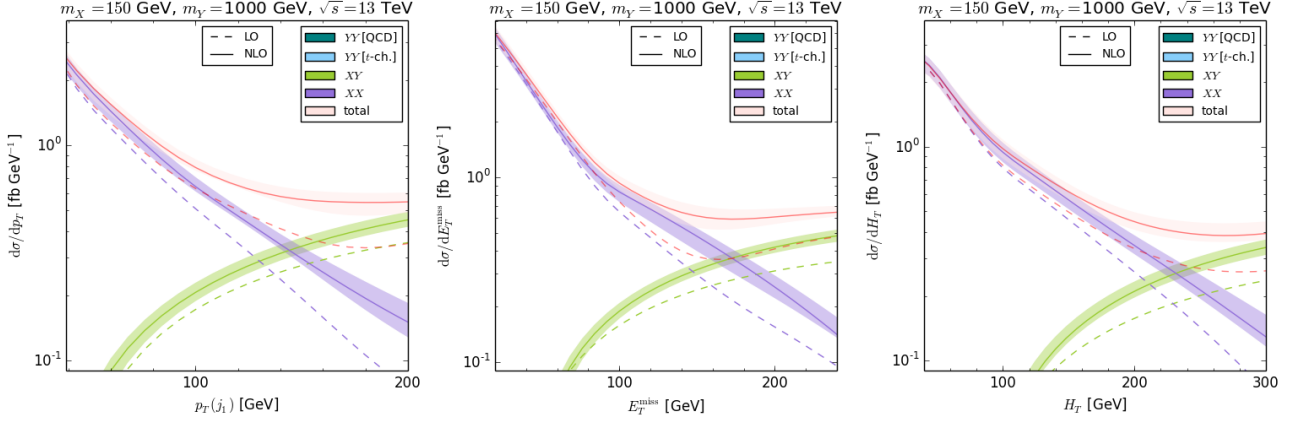


**Fig. 4** Same as figure 3 but for the **S2** scenario.

respond to the uncertainty bands obtained as described above, *i.e.* from a nine-point variation of the unphysical factorisation and renormalisation scales.

Our results show that the dark matter pair-production channel, despite a large production cross section (see table 4), mainly yields events featuring a small amount of missing energy and not so much hadronic activity, even if at the matrix-element level, our simulation includes a selection cut of 100 GeV on the  $p_T$  of the leading (parton-level) jet. After matching the fixed-order NLO predictions with parton showers, the emissions originating from this hard parton are often not reclustered back so that a small ensemble of softer jets are finally reconstructed from the initial hard radiation. Consequently, the dark matter particles turn out to be mostly produced back-to-back, which leads to a small amount of missing energy, and in association with a small hadronic activity. As a consequence, the efficiency of a typical monojet selection is expected to

be quite reduced as one generally requires a substantial amount of missing energy and hadronic activity. We refer to section 3.4 for more details.

The leading relevant process from the cross sections presented in table 4 therefore consists in the associated production of a dark matter particle with a heavier mediator  $pp \rightarrow XY$ . The  $Y \rightarrow Xq$  decay of the mediator leads to the production of a second dark matter state together with a hard parton, which guarantees a much larger missing transverse energy and hadronic activity than for the  $pp \rightarrow XX$  channel. The results, depicted by the green curves in figures 3 and 4 for the **S1** and **S2** scenarios respectively, confirm this, the corresponding  $E_T^{\text{miss}}$ ,  $p_T(j_1)$  and  $H_T$  distributions being depleted in the low-energy regime. In the high-energy tails, the  $XY$  contributions moreover almost match entirely the total new physics signal (red curves), the  $pp \rightarrow YY$  contributions being only expected to take over in the very hard part of the phase space (not represented in

figure 3 and that is drastically phase-space-suppressed, and thus not shown, for the **S2** setup in figure 4). The  $XY$  distributions are indeed steeply falling with the energy scale, compared with the  $YY$  ones, so that the  $XY$  component of the signal is only dominant for moderate observable values of a few hundreds of GeV. The relative importance of the  $XY$  process can however be tamed down by reducing the magnitude of the  $\lambda_\varphi$  coupling, on which the normalisation of the distributions depends quadratically as the amplitude of the corresponding partonic process  $qg \rightarrow XY$  is linear in both the new physics and strong coupling constants (see the right diagram in figure 1).

Finally, mediator pair production ( $pp \rightarrow YY$ ) only dominates, as said above, in the harder part of the spectra where all other contributions are kinematically suppressed. In that regime, the decays of the two heavy mediators into  $Xq$  systems guarantee an amount of missing energy and hadronic activity greater than for  $XY$  production, despite the global rates being reduced by the large mediator mass. In our analysis, we distinguish the QCD production mode whose matrix element is proportional to  $\alpha_s^2$  and independent of  $\lambda_\varphi$ , and the  $t$ -channel one that depends on  $\lambda_\varphi^4$ . Whereas for the adopted  $\lambda_\varphi = 1$  benchmark value, the two production channels contribute equivalently, the  $t$ -channel impact can be reduced by fixing  $\lambda_\varphi$  to a smaller value. For  $\lambda_\varphi \sim g_w$  ( $g_w$  being the weak coupling constant), we obtain the widely studied supersymmetric limiting scenario in which all superpartners except the right-handed up squark and a bino-like neutralino are decoupled, with a difference on the dark matter nature that is here a Dirac fermion. In this case, only the QCD production of two mediators matters, and the  $t$ -channel contribution to  $YY$  production and  $XY$  production can be ignored (at least for the considered mediator masses).

### 3.4 Collider constraints on S3D\_uR dark matter

As visible from the results of section 3.3, most of the monojet signal arises, in the considered **S1** and **S2** benchmark scenarios, from the production of heavy mediators (by pairs or in association with dark matter) that then decay into dark matter and jets. In the following, we reinterpret the results of typical LHC dark matter searches probing final states featuring a large amount of missing transverse energy (carried away by the dark matter particles) and an important hadronic activity. We recast two of such ATLAS analyses for which reimplementations within the MADANALYSIS 5 Public Analysis Database (PAD) of recasted LHC anal-

yses [56]<sup>2</sup> exist. Starting from Monte Carlo simulations of the  $XX + XY + YY$  dark matter signal as described in section 3.2, we make use of MADANALYSIS 5 to automatically simulate the response of the ATLAS detector by means of appropriate tunes of the DELPHES 3 programme [57]. We then assess the sensitivity of the considered analyses to the **S1** and **S2** signals by using the CL<sub>s</sub> method [58].

We consider two ATLAS analyses of 36.2 fb<sup>-1</sup> of LHC data targeting the production of missing energy recoiling against at least one hard jet and a subleading hadronic activity. We recast the ATLAS-EXOT-2016-27 analysis [51–53] in which the selection imposes that the dark matter system is produced together with 2 to 4 extra hard jets with quite stringent kinematic requirements. The analysis includes an ensemble of signal regions that are distinguished by different inclusive and exclusive constraints on the missing transverse energy. In the ATLAS-SUSY-2016-07 analysis [54, 55], a larger number of jets  $N_j$  is allowed ( $N_j \geq 2$ ) and the properties of those jets are less constrained. The analysis includes several signal regions that mainly differ by the minimum number of required jets and a constraint on the effective mass  $M_{\text{eff}}$  defined by

$$M_{\text{eff}} = E_T^{\text{miss}} + \sum_{\text{jets}} p_T. \quad (18)$$

Our results are presented in tables 5 and 6 for the ATLAS-EXOT-2016-27 and ATLAS-SUSY-2016-07 analysis, respectively. In each table, we show the confidence level (CL) exclusion obtained when the analysis signal regions are populated by all the  $XX$ ,  $XY$  and  $YY$  contributions to the signal. The impact of the individual channels is also reported, the  $YY$  component being further decomposed into its QCD and  $t$ -channel part. Our results include theoretical scale uncertainties, which we have extracted by propagating the uncertainties on the total cross sections down to the CL<sub>s</sub> exclusions that we have computed both at LO and NLO. In our recasting procedure, we conservatively make use of the most sensitive signal region of each analysis, to derive the exclusion levels, as the statistical model used by the ATLAS collaboration for the combination of the various regions is not publicly available. The definition of these regions is provided in the tables, that hence include the required  $E_T^{\text{miss}}$  range for the ATLAS-EXOT-2016-27 analysis, and the thresholds on  $N_j$  and  $M_{\text{eff}}$  for the ATLAS-SUSY-2016-07 analysis.

It turns out that both the **S1** and **S2** scenarios are excluded at the 95% CL by both analyses, even after

<sup>2</sup>See the URL <http://madanalysis.irmp.ucl.ac.be/wiki/PublicAnalysisDatabase>.

Sc.	Process	CL <sub>s</sub> [LO]	$E_T^{\text{miss}}$ constraint	CL <sub>s</sub> [NLO]	$E_T^{\text{miss}}$ constraint
<b>S1</b>	Total	100 %	$\in [300, 350]$ GeV	100 %	$\in [300, 350]$ GeV
	XX	$1.6^{+0.2}_{-0.1}$ %	$\in [300, 350]$ GeV	$9.4^{+0.6}_{-0.6}$ %	$\in [250, 300]$ GeV
	XY	100 %	$\in [300, 350]$ GeV	100 %	$\in [300, 350]$ GeV
	YY [total]	$91.3^{+6.2}_{-8.8}$ %	$\in [300, 350]$ GeV	100 %	$\in [300, 350]$ GeV
	YY [QCD]	$63.0^{+20.0}_{-17.2}$ %	$\in [300, 350]$ GeV	$88.3^{+4.8}_{-7.4}$ %	$\in [300, 350]$ GeV
	YY [ <i>t</i> -channel]	$70.8^{+5.0}_{-4.6}$ %	$\in [300, 350]$ GeV	$87.2^{+1.0}_{-1.4}$ %	$\in [300, 350]$ GeV
<b>S2</b>	Total	$75.6^{+10.1}_{-10.5}$ %	$\in [700, 800]$ GeV	$97.8^{+0.9}_{-1.4}$ %	$\geq 700$ GeV
	XX	$0.7^{+0.6}_{-0.6}$ %	$\in [250, 300]$ GeV	$3.6^{+0.3}_{-0.6}$ %	$\geq 900$ GeV
	XY	$62.7^{+12.3}_{-10.4}$ %	$\in [500, 600]$ GeV	$83.9^{+2.9}_{-4.3}$ %	$\in [700, 800]$ GeV
	YY [total]	$24.0^{+3.1}_{-3.1}$ %	$\geq 900$ GeV	$58.1^{+2.2}_{-3.1}$ %	$\geq 900$ GeV
	YY [QCD]	$10.7^{+4.4}_{-2.6}$ %	$\geq 900$ GeV	$17.0^{+2.1}_{-2.1}$ %	$\geq 900$ GeV
	YY [ <i>t</i> -channel]	$29.6^{+3.3}_{-2.6}$ %	$\geq 900$ GeV	$38.9^{+1.2}_{-1.8}$ %	$\geq 900$ GeV

**Table 5** *CL* exclusions obtained from MADANALYSIS 5 by recasting the ATLAS-EXOT-2016-27 analysis [51–53]. The uncertainties are given as absolute quantities and originate from scale variations only. When omitted, the result is independent of the scale uncertainties. We also indicate the  $E_T^{\text{miss}}$  requirement defining the most sensitive signal region.

Sc.	Process	CL <sub>s</sub> [LO]	$N_j$	$M_{\text{eff}}$ threshold	CL <sub>s</sub> [NLO]	$N_j$	$M_{\text{eff}}$ threshold
<b>S1</b>	Total	$99.5^{+0.4}_{-2.1}$ %	$\geq 4$	$> 1.4$ TeV	100 %	$\geq 5$	$> 2$ TeV
	XX	$0.6^{+0.6}_{-0.6}$ %	$\geq 5$	$> 1.7$ TeV	$3.3^{+0.1}_{-0.3}$ %	$\geq 2$	$> 1.6$ TeV
	XY	$89.2^{+4.5}_{-4.8}$ %	$\geq 2$	$> 1.6$ TeV	$99.8^{+0.1}_{-0.2}$ %	$\geq 5$	$> 2$ TeV
	YY [total]	$96.0^{+3.4}_{-7.6}$ %	$\geq 4$	$> 1.4$ TeV	$97.2^{+1.4}_{-2.6}$ %	$\geq 4$	$> 1.4$ TeV
	YY [QCD]	$88.7^{+8.8}_{-14.5}$ %	$\geq 4$	$> 1.4$ TeV	$93.7^{+2.7}_{-5.2}$ %	$\geq 4$	$> 1.4$ TeV
	YY [ <i>t</i> -channel]	$35.1^{+3.4}_{-2.1}$ %	$\geq 4$	$> 1.4$ TeV	$29.7^{+0.2}_{-1.4}$ %	$\geq 5$	$> 2$ TeV
<b>S2</b>	Total	$95.0^{+3.0}_{-4.3}$ %	$\geq 2$	$> 1.6$ TeV	100 %	$\geq 2$	$> 1.6$ TeV
	XX	$0.6^{+0.6}_{-0.6}$ %	$\geq 6$	$> 2.2$ TeV	$1.0^{+0.0}_{-0.2}$ %	$\geq 3$	$> 1.3$ TeV
	XY	$61.7^{+8.4}_{-7.0}$ %	$\geq 2$	$> 1.6$ TeV	$83.6^{+1.5}_{-3.1}$ %	$\geq 2$	$> 2$ TeV
	YY [total]	$77.4^{+7.9}_{-7.5}$ %	$\geq 2$	$> 1.6$ TeV	$97.8^{+0.5}_{-1.1}$ %	$\geq 2$	$> 1.6$ TeV
	YY [QCD]	$55.3^{+12.0}_{-12.3}$ %	$\geq 2$	$> 2$ TeV	$67.7^{+4.1}_{-6.4}$ %	$\geq 2$	$> 1.6$ TeV
	YY [ <i>t</i> -channel]	$75.6^{+4.4}_{-4.8}$ %	$\geq 2$	$> 2$ TeV	$80.1^{+0.3}_{-1.6}$ %	$\geq 2$	$> 1.6$ TeV

**Table 6** Same as in table 5 but for the ATLAS-SUSY-2016-07 analysis [54, 55]. We indicate here the jet multiplicity requirement and the effective mass  $M_{\text{eff}}$  threshold defining the most sensitive signal region.

accounting for the uncertainties on the total rates. However, such a conclusion can only be drawn when more precise NLO simulations are employed and after summing over the XX, XY and YY contributions. As already detailed in section 3.3, we have found that dark matter pair production plays no role in the exclusion.

The associated production of a mediator and a dark matter particle (XY) has the largest impact on the

ATLAS-EXOT-2016-27 exclusion, the analysis excluding the **S1** model by solely using this component of the signal. This stems from an exclusive region in which

$$300 \text{ GeV} \leq E_T^{\text{miss}} < 350 \text{ GeV} . \quad (19)$$

Such a range corresponds to a phase-space region containing a significant fraction of the  $pp \rightarrow XY$  events

(see figure 3). The sensitivity to the **S2** scenario, featuring a much heavier mediator ( $m_Y = 1$  TeV), is found to be slightly below  $2\sigma$  when using NLO simulations. In contrast, LO predictions lead to too conservative conclusions, with a sensitivity barely reaching the  $1\sigma$  level. The LO results are additionally plagued with large scale uncertainties. The NLO corrections also affect the shapes, and different signal regions are the most sensitive ones to the LO and NLO signals,

$$\begin{aligned} \text{LO : } 500 \text{ GeV} &\leq E_T^{\text{miss}} < 600 \text{ GeV} , \\ \text{NLO : } 700 \text{ GeV} &\leq E_T^{\text{miss}} < 800 \text{ GeV} . \end{aligned} \quad (20)$$

The  $pp \rightarrow YY$  production cross section being smaller, the sensitivity of the ATLAS-EXOT-2016-27 analysis to this channel is expected to be reduced, although the final-state objects that are typically reconstructed are significantly harder due to the production of two heavy mediators. In the **S1** scenario, this effect is irrelevant as the mediator is light enough ( $m_Y = 500$  GeV) to be copiously pair-produced. The subsequent signal is hence excluded by the same signal region as the one defined in eq. (19). Such a statement can however only be made after using NLO simulations (the LO rates being too small to reach a 95% CL exclusion) and when including not only the QCD-induced production mode, but also the dark matter  $t$ -channel exchange one. In the case of the **S2** scenario, the signal regions are not populated enough to exclude the model. However, the yields are sufficiently large for driving an exclusion by considering both the  $YY$  and  $XY$  contributions, again provided NLO simulations are used.

We derive similar conclusions from the results obtained by recasting the ATLAS-SUSY-2016-07 analysis. This analysis, that involves more complex cuts, better depicts the NLO impact on the shapes of the differential distributions. The corresponding modifications at the differential level indeed often lead to consider different most sensitive regions at LO and NLO.

With the examples worked out in this section, we have demonstrated the importance of relying on new physics precision simulations including NLO QCD predictions matched with parton showers. The correspondingly more precisely known total and differential cross sections allow for more robust conclusions on the sensitivity to the signal. The differences at the level of the distributions especially play a significant role in modifying the way in controlling how the different signal regions of the LHC analyses are populated. Moreover, it is crucial to consider all the components of a given signal, as their joint contribution may be sufficient to claim an exclusion, in contrast to the individual contributions taken separately.

## 4 Dark matter observables in $t$ -channel models

### 4.1 Generalities

The studied  $t$ -channel simplified models are very peculiar as far as their dark matter phenomenology is concerned. While tree-level cross sections can be negligible, if not zero, NLO corrections or loop-induced processes might set up the stage. This is the case for any considered model restriction involving Majorana or scalar dark matter [18–20, 32, 59, 60], while it is more model dependent for Dirac dark matter [21]. In the following, we focus on the fermionic dark matter case. In the early universe, the relic abundance is set by the annihilation of  $\tilde{\chi}\tilde{\chi}$  (Majorana) or  $\chi\bar{\chi}$  (Dirac) pairs (see the left diagram in figure 5), unless the mediator  $\varphi$  and the dark matter are within 20% in mass ( $r \equiv M_\varphi/M_\chi \lesssim 1.2$ ). In this case, coannihilations [61] should be included as they dominate over a wide range of the parameter space (see the central and right diagrams in figure 5). Moreover, our analysis does not include Sommerfeld enhancement effects [62, 63], as they are known not to alter the relic density predictions by more than 15% and only affect specific parts of the parameter space [20, 64–66].

We first consider, as in section 3, a model restriction in which Dirac dark matter solely couples to the right-handed up quark (S3D.uR). In this model, both the dark matter spin-independent (SI) and spin-dependent (SD) elastic scattering cross sections off nucleons feature sizeable tree-level contributions stemming from  $s$ -channel mediator exchanges. When coannihilations are negligible ( $r \gtrsim 1.2$ ), indirect detection rates stem from  $\chi\bar{\chi}$  annihilations into pairs of right-handed up quarks, which proceeds via  $s$ -wave  $t$ -channel mediator exchanges. The associated velocity-averaged cross section is about  $3 \times 10^{-26} \text{ cm}^3/\text{s}$  for large  $\lambda_\varphi$  values, and thus in the ballpark of the reach of the Fermi-LAT gamma-ray searches from dwarf spheroidal galaxies [67]. For illustrative purposes, we discuss, in the following, relic density and direct detection predictions. We refer to refs. [21, 25, 27] for more comprehensive studies.

The Majorana dark matter restriction (S3M.uR) is similar to a supersymmetric model with bino-like neutralino dark matter and a right-handed up squark mediator. In this configuration, predictions for direct and indirect detection observables are dictated by NLO QCD corrections and loop-induced processes respectively. The direct detection SI elastic scattering cross section is negligible at tree level because of the Majorana nature of the dark matter, for which vectorial currents vanish. NLO QCD contributions at one loop, that include diagrams involving quarks and scalar mediators, therefore dominate and drive the scattering of dark matter off

the nucleon constituents [22, 23, 68–71]. The SD elastic scattering cross section is, on the contrary, dominantly dominated by tree-level contributions, and can be of the same order as the current experimental sensitivity.

Present day  $\tilde{\chi}\tilde{\chi} \rightarrow u\bar{u}$  annihilations in dense astrophysical environments are  $p$ -wave suppressed, as the tree-level  $s$ -wave contribution is proportional to the up-quark mass that vanishes in the chiral limit. There however exist two processes that could make Majorana dark matter detectable: virtual internal bremsstrahlung (VIB) in which the quark pair is produced together with a photon emitted by the internal  $t$ -channel propagator, and loop-induced annihilations into a photon pair or into a photon and a  $Z$ -boson. VIB yields a large correction to the tree-level annihilation cross section, uplifting the  $p$ -wave suppression by even a few orders of magnitude, and provides a sharp spectral feature at the highest end of the gamma-ray spectrum (see, *e.g.*, refs. [18–20, 59, 65, 66, 72–74]). On the other hand, annihilations into photons have been known since a long time as the smoking gun to detect dark matter, as they produce monochromatic photons pinpointing the dark matter mass (see, *e.g.*, refs. [75–80]). Whilst these two processes are of higher order, the astrophysical background for a sharp gamma-ray spectral feature is very low. This yields a very good experimental sensitivity and annihilation cross sections well below the canonical  $10^{-26} \text{ cm}^3/\text{s}$  value can be probed for a wide range of dark matter masses [81]. Moreover, line searches by the HESS satellite [82, 83] are sensitive to very heavy dark matter, with masses of tens of TeV, well above the sensitivity range of the LHC. This thus exhibits a nice complementarity with colliders.

The Majorana dark matter phenomenology briefly sketched here holds for scalar dark matter too. NLO processes even become relevant at freeze-out, the tree-level annihilation cross section being  $d$ -wave suppressed [59]. Similarly, any  $t$ -channel dark matter model restriction in which the dark matter couples only to the third generation requires to account for QCD corrections already for the relic density predictions [60]. For instance, for all restrictions of the 3rd type, loop-induced dark matter annihilations into gluons turn out to be dominant and set the relic density below the  $b$ -quark threshold [84]. These corrections are typically not automatically included in available public software such as MADDM and MICROMEAS, and must be implemented following, *e.g.*, refs. [59, 84].

#### 4.2 Analysis setup and validation procedure

In our dark matter analysis, we impose the relic abundance for dark matter to match the value measured by

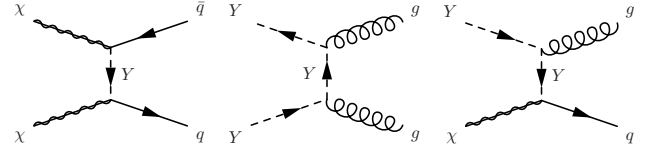


**Fig. 5** Representative LO Feynman diagrams entering the relic density computation. We consider dark matter annihilations into quarks (left), as well as mediator annihilations (centre) and coannihilations (right) that are relevant for mediator and dark matter mass splittings of about 10–20%.

the Planck satellite in 2018 [85]. The direct detection predictions are confronted with the exclusion bounds at 90% CL of the XENON1T [86] and of PICO-60 [87] experiments for the SI and SD cases respectively, and we display projections for the neutrino floor in our SI scattering results [88]. Loop-induced gamma-ray line predictions are compared with the Fermi-LAT [81] and HESS [82, 83] line searches from the galactic centre, as recasted in ref. [17] for an Einasto dark matter density profile [89] at 95% CL. We also show the projected sensitivity of the Cherenkov Telescope Array (CTA) [90] as obtained in ref. [17] at 95% CL.

In order to compute the relevant observables with MADDM in the S3D\_uR model restriction, we type in the command line interface of the programme,

```
import model DMSimp_t-S3D_uR --modelname
define darkmatter xd
define coannihilator ys3u1
generate relic_density
add direct_detection
output my_project
launch
```

In the case of Majorana dark matter, the model name should be changed to DMSimp\_t-S3M\_uR, and the dark matter candidate name to xm (see table 1). Scans can be performed by using standard MADDM syntax [6], and details for indirect detection calculations are provided in the next subsections. Representative Feynman diagrams contributing to the thermally-averaged annihilation cross section  $\langle\sigma v\rangle_{\text{fo}}$ , assuming a standard dark matter freeze-out (fo), are depicted in figure 5.

To achieve our calculations in MADDM, we produce a LO UFO library in which all quarks are massive (unless stated otherwise). It differs from the NLO UFO library described in section 2.1 in which all quarks except the top quark are massless. We moreover have additionally generated CALCHEP model files [91], which is necessary to validate MADDM predictions obtained with the DMSimp model against known results [18, 19, 59] derived with MICROMEAS. All model files are available from the URL <http://feynrules.irmp.ucl.ac.be/wiki/DMSimp>.



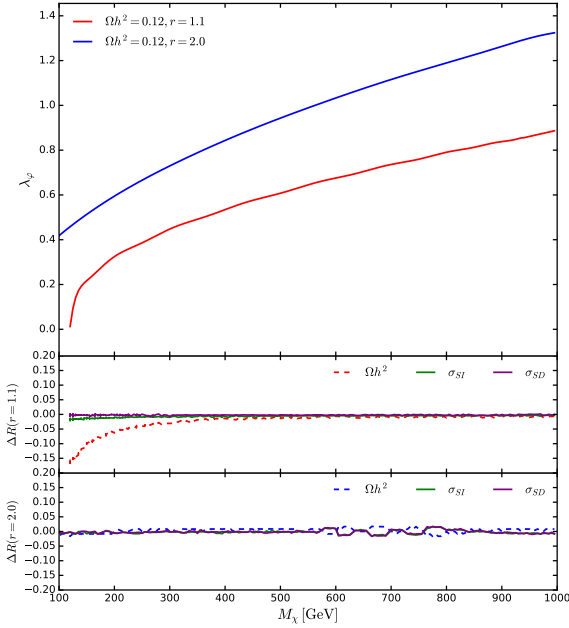


**Fig. 6** Value of the  $\lambda_\varphi$  coupling, as a function of the dark matter mass  $M_\chi$ , leading to a relic density of  $\Omega h^2 = 0.12$  in the S3D\_uR model (top). We present MICROMEGAS predictions for  $r=1.1$  (red) and 2 (blue). We moreover display the relative difference between MICROMEGAS and MADDM for the relic density (dashed), the SI (solid green) and SD (solid magenta) scattering cross section off protons for  $r=1.1$  (centre) and 2 (bottom).

#### 4.3 Dark matter observables in the S3D\_uR model

In figure 6, we validate our S3D\_uR model implementation by numerically comparing relic density and direct detection predictions obtained with MADDM and MICROMEGAS. In the upper panel, we derive the  $\lambda_\varphi$  coupling value required to obtain the correct relic density as a function of the dark matter mass, for two choices of the mediator and dark matter mass ratio  $r$ .

In the more compressed scenario with  $r=1.1$  (red curve), coannihilations and mediator annihilations are important, especially for small  $M_\chi$ . For  $M_\chi \lesssim 200$  GeV, the relic density is indeed mostly independent of  $\lambda_\varphi$ ,  $\langle\sigma v\rangle_{\text{fo}}$  being driven by pure QCD processes involving pairs of mediators annihilating into quarks and gluons (second diagram in figure 5). To properly evaluate these QCD processes, we include the running of the strong coupling in MADDM<sup>3</sup>, as implemented by default in MG5\_AMC [92]. The number of quarks included in the loops depends on the running scale (and can be at most 5), and the QCD beta function can be evaluated at 1,

<sup>3</sup>This feature is now standard in the publicly available version of MADDM at the URL <https://launchpad.net/maddm>.

2 (default) and 3 loops. As far as the dark matter mass increases, processes involving both  $\chi$  and  $\varphi$  become relevant so that  $\lambda_\varphi$  has to be sizeable to obtain the right relic density. Already for  $M_\chi \sim 250$  GeV,  $XX$  annihilations (first diagram in figure 5) and  $XY$  coannihilations (third diagram in figure 5) contribute to the total scattering cross section  $\langle\sigma v\rangle_{\text{fo}}$  by about 45% and 30% respectively, the reminder being due to mediator-pair annihilations ( $YY$ ). As in the previous section,  $X=\chi, \bar{\chi}$  and  $Y=\varphi, \varphi^\dagger$  in our notations. For dark matter masses larger than 500 GeV,  $XX$  annihilations dominate, the  $XY$  and  $YY$  processes contributing only to less than about 20% to the relic density.

In the  $r=2$  case (blue line),  $Y$  is too heavy relatively to dark matter to be relevant at freeze-out. Only  $XX$  annihilations contribute, and  $\lambda_\varphi$  has to be sizeable and larger than for  $r=1.1$  for any a given  $M_\chi$  value. This large value compensates the smaller  $\langle\sigma v\rangle_{\text{fo}}$  cross section stemming from a smaller number of relevant processes than in the  $r=1.1$  scenario where coannihilations and mediator annihilations play a role.

In order to quantify the numerical differences between MICROMEGAS and MADDM predictions for a given dark matter observable  $\mathcal{O}$ , we define the quantity

$$\Delta R = \frac{\mathcal{O}_{\text{MICROMEGAS}} - \mathcal{O}_{\text{MADDM}}}{\mathcal{O}_{\text{MICROMEGAS}}} . \quad (21)$$

and focus, in figure 6, on the relic density (dashed), and the SI (solid green) and SD (solid magenta) direct detection cross sections. We present the dependence of  $\Delta R$  on the dark matter mass both for the  $r=1.1$  (middle panel) and  $r=2$  (lower panel) scenarios. Predictions for both the SI and SD dark matter scattering cross section off protons<sup>4</sup> are found in perfect agreement, the discrepancy between MADDM and MICROMEGAS being of at most a few percents for the probed dark matter mass range. Relic density predictions are also found to agree quite well, except for dark matter masses in the 100–200 GeV range for the  $r=1.1$  configuration. In this parameter space region, we get a discrepancy reaching 5% to 15% due to the different treatment of the QCD sector in both codes (the relic density being driven by QCD-induced mediator annihilations). MICROMEGAS indeed includes running quark masses, in addition to the strong coupling running [93].

#### 4.4 Dark matter observables in the S3M\_uR model

In this section, we focus on Majorana dark matter and derive, in figure 7, the values of the  $\lambda_\varphi$  coupling that are needed to obtain the correct relic density for  $r=1.1$

<sup>4</sup>Similar results are obtained in the neutron case.

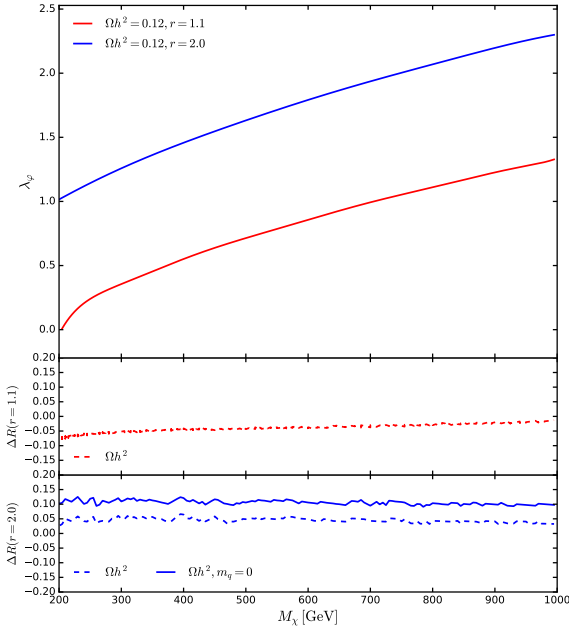


**Fig. 7** Value of the  $\lambda_\phi$  coupling, as a function of the dark matter mass  $M_\chi$ , leading to a relic density of  $\Omega h^2 = 0.12$  in the S3M\_uR model (top). We present MICROMEGAS predictions for  $r=1.1$  (red) and 2 (blue). We moreover display the relative difference between MICROMEGAS and MADDM for the relic density (dashed) for  $r=1.1$  (centre) and 2 (bottom). In the last case, the limits in which all quarks are massless are also presented (solid).

(red) and  $r=2$  (blue) configurations. Comparing with the Dirac dark matter case, larger couplings are generally required as a consequence of the Majorana nature of dark matter, with the exception of setups featuring dark matter masses below 500 GeV where the relic density is driven by mediator annihilations and coannihilations. Another remarkable difference with Dirac dark matter, in the  $r=1.1$  scenario, is that there is no phenomenologically-viable solution for  $M_\chi \lesssim 200$  GeV. In the middle and lower panel of the figure, we show that MADDM and MICROMEGAS predictions agree quite well, as  $\Delta R \lesssim 5\%$  for both scenarios (dashed lines), except for light dark matter where more important differences stem from the different treatment of the QCD sector. We additionally assess the impact of the quark masses that induce a 10% shift (including running quark mass effects) relatively to the values obtained with MICROMEGAS (for a massive quark setup).

In figure 8, we estimate the NLO SI dark matter elastic scattering cross section off protons for the  $r=1.1$  (red) and  $r=2$  (blue) scenarios. For each dark matter mass value, we fix the  $\lambda_\phi$  coupling to reproduce the

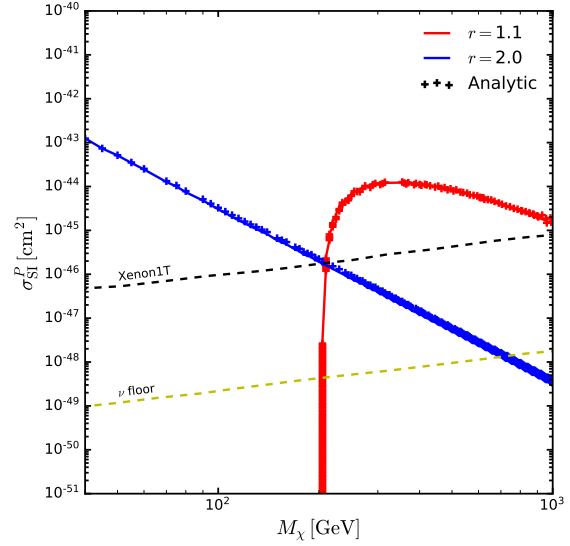


**Fig. 8** NLO SI scattering cross section off protons as a function of the dark matter mass for  $r=1.1$  (red) and  $r=2$  (blue), with a  $\lambda_\phi$  coupling yielding the right relic density. We compare MICROMEGAS predictions (solid lines) with the analytical results of ref. [23]. We additionally include the exclusion bounds extracted from current XENON1T results [86] (dashed black line) and the neutrino floor [88] (dashed yellow line).

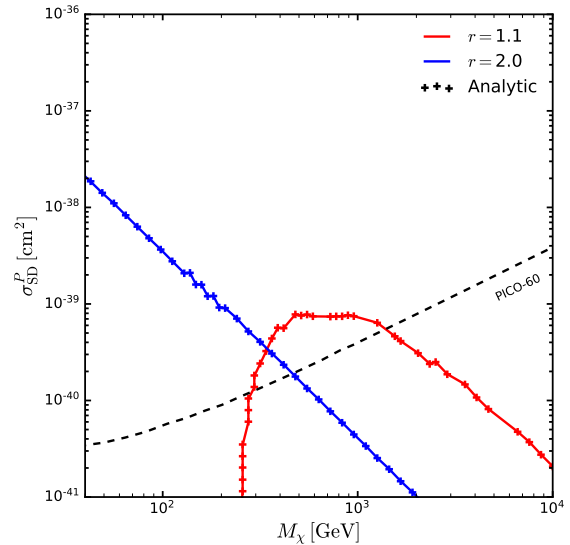


**Fig. 9** Same as figure 8 but for the SD scattering cross section. The predictions are compared with the current PICO-60 exclusion bounds [87] (dashed black line).

relic density as observed by the Planck collaboration. We compare predictions obtained with MICROMEGAS (solid curves) with the sum (markers) of the MADDM LO results and the analytically available NLO corrections [23]. An excellent agreement is found. Confronting those results to the exclusion limits of XENON1T [86],

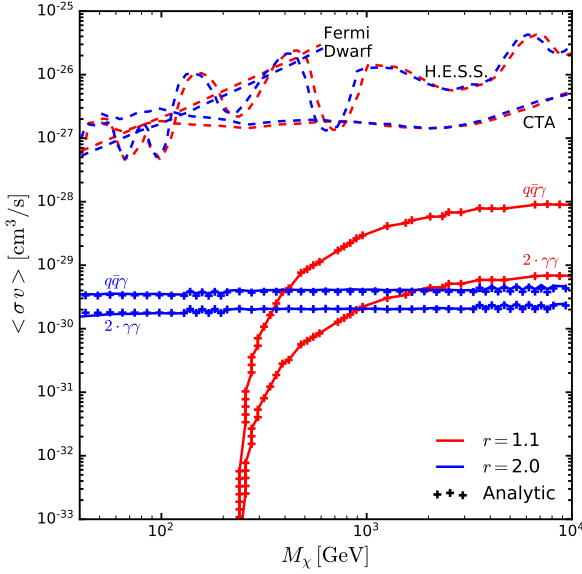


**Fig. 10** Present time dark matter annihilation cross section as a function of  $M_\chi$  in the  $r = 1.1$  (red) and  $r = 2$  (blue) configurations. Predictions for the VIB ( $q\bar{q}\gamma$ ) and photon-pair production ( $\gamma\gamma$ ) modes have been automatically computed with MADDM, and compared with the analytic expressions of refs. [18] and [59] for the VIB and  $\gamma\gamma$  processes respectively. We additionally show constraints (dashed) from the Fermi-LAT dwarf spheroidal galaxies measurements and from the HESS experiment [17], as well as the expected sensitivity of the CTA experiment [17].

half of the viable parameter space ( $M_\chi \lesssim 150$  GeV) is excluded for both spectrum compression options. Moreover, this shows that most of the currently viable parameter space can be explored by next-generation dark matter experiments, as the corresponding SI scattering cross sections are larger than the expectation of the neutrino background [88].

Predictions for the LO SD elastic dark matter cross section off protons are shown in figure 9, in which we demonstrate the agreement between the numerical results of MADDM (solid lines) and the analytic expressions of ref. [23] (markers). Confronting those predictions with the exclusion limits obtained from the PICO-60 experiment [87], it turns out that dark matter masses smaller than 500 GeV in the  $r = 2$  configuration, and lying in the [250, 1200] GeV range in the  $r = 1.1$  case, are disfavoured. Whereas the running of the  $\lambda_\varphi$  coupling from the electroweak scale down to the GeV scale is known to largely enhance direct detection cross section predictions [32], this effect is not included neither in MADDM nor in MICROMEAS. This goes beyond the scope of this work.

We finally consider dark matter indirect detection in figure 10, in which we present predictions for the present time dark matter annihilation cross section in

the  $\tilde{\chi}\tilde{\chi} \rightarrow u\bar{u}\gamma$  and  $\tilde{\chi}\tilde{\chi} \rightarrow \gamma\gamma$  channels for both considered benchmark scenarios. In both cases, the VIB cross section is larger than the diphoton one, although the latter loop-induced rate is of a similar order of magnitude as the former three-body one<sup>5</sup>. For more split spectra, or equivalently for larger  $r$  values, the loop-induced contributions are however known to dominate [19]. Confronting our predictions with the experimental results that are very sensitive to sharp features and lines in the gamma-ray spectra, we observe that there is no sensitivity to the two considered benchmark scenarios. This holds both for current exclusions extracted from the Fermi-LAT dwarf spheroidal galaxy measurements or HESS data, and for the expectation of the future CTA line search from the galactic centre.

In our predictions, we have compared the results of MADDM obtained by using the NLO DMSimp UFO library of section 2.1 (solid lines) with the analytical approximated expressions of refs. [18] and [59] for the VIB and diphoton channels, respectively. As discussed in the manual [6], MADDM can automatically handle  $2 \rightarrow 3$  generic annihilation processes by typing in,

```
import model DMSimp_t-S3M_uR --modelname
define darkmatter xm
define coannihilator ys3u1
generate indirect_detection u u~ a
output my_project
launch
```

The results of figure 10 however represents the first validation of a fully automated loop-induced process computation for a dark matter observable. This feature will be available from the future version of MADDM<sup>6</sup>.

## 5 Summary and conclusion

In this work, we have introduced the DMSimp framework for dark matter  $t$ -channel models, available from the URL <http://feynrules.irmp.ucl.ac.be/wiki/DMSimp>. This consists in a unique FEYNRULES implementation that allows for the calculation, through the various high-energy physics tools interfaced to FEYNRULES, of a large set of dark matter observables at colliders and in cosmology. The model is shipped with several restrictions relevant for simplified models featuring dark matter and coloured mediators of different spins. We have extensively studied two of those restrictions in which the dark matter is either a Dirac or a Majorana fermion, and the mediator is a scalar state coupling to the right-handed up quark.

<sup>5</sup>The extra factor of two accounts for the photon multiplicity.

<sup>6</sup>This release can already be obtained from the authors.

We have generated a UFO model including ingredients for the automatic computation of collider observables matching NLO QCD predictions with parton showers. By a joint use of the MG5\_AMC, PYTHIA 8, MADANALYSIS 5, FASTJET and DELPHES 3 programmes, we have investigated the impact of the NLO corrections on various observables relevant for typical dark matter searches at the LHC through monojet probes, and shown how this could affect the sensitivity of the corresponding experimental searches. Our results emphasise the benefits of using NLO simulations to get more realistic predictions for total and differential cross sections including smaller theoretical systematics. We have moreover demonstrated how considering all new physics signals predicted by a given scenario as a whole is necessary for a better assessment of the LHC sensitivity to new phenomena. At the NLO accuracy, this however requires a specific treatment of  $s$ -channel resonant contributions usually appearing in the real emission contributions in order to avoid their double counting. Such a task can be automatically achieved within the MG5\_AMC framework.

We have then made use of the MADDM programme for the automatic calculation of the dark matter relic density, spin-independent and spin-dependent scattering cross sections off nucleons and indirect detection rates. We have validated our predictions through a comparison with MICROMEGAS (using a CALCHEP model file generated from our general DMSimpT FEYNRULES implementation) and existing analytical calculations. Our predictions include both NLO corrections and the contributions of loop-induced processes as they could be dominant in specific model configurations, in particular for what concerns Majorana dark matter spin-independent direct detection (that is strongly affected by higher orders) and indirect detection (driven by loop-induced and virtual internal bremsstrahlung subprocesses). While MICROMEGAS can account for corrections to direct detection, MADDM can automatically evaluate VIB processes. We have moreover pioneered the first automatic calculation of a loop-induced contribution to the production of gamma-ray lines by dark matter annihilations at present time.

In conclusion, our work presents, for the first time, a unified framework to undertake precision dark matter calculations in cosmology and at colliders for a large class of  $t$ -channel dark matter models.

**Acknowledgements** The authors are grateful to L. Lopez Honorez, K. Mohan, A. Pukhov and T. Tait for their help and useful comments during the model validation steps. CA is supported by the Innoviris ATTRACT 2018 104 BECAP 2 agreement. This work has received funding from the European Union's Horizon 2020 research and innovation pro-

gramme as part of the Marie Skłodowska-Curie Innovative Training Network MCnetITN3 (grant agreement no. 722104).

## References

1. J. Silk et al., *Particle Dark Matter: Observations, Models and Searches*. Cambridge Univ. Press, Cambridge, 2010, [10.1017/CBO9780511770739](#).
2. J. Alwall, P. Schuster and N. Toro, *Simplified Models for a First Characterization of New Physics at the LHC*, *Phys. Rev. D* **79** (2009) 075020 [[0810.3921](#)].
3. LHC NEW PHYSICS WORKING GROUP collaboration, *Simplified Models for LHC New Physics Searches*, *J. Phys. G* **39** (2012) 105005 [[1105.2838](#)].
4. A. Alloul, N. D. Christensen, C. Degrande, C. Duhr and B. Fuks, *FeynRules 2.0 - A complete toolbox for tree-level phenomenology*, *Comput. Phys. Commun.* **185** (2014) 2250 [[1310.1921](#)].
5. J. Alwall, R. Frederix, S. Frixione, V. Hirschi, F. Maltoni, O. Mattelaer et al., *The automated computation of tree-level and next-to-leading order differential cross sections, and their matching to parton shower simulations*, *JHEP* **07** (2014) 079 [[1405.0301](#)].
6. F. Ambrogio, C. Arina, M. Backovic, J. Heisig, F. Maltoni, L. Mantani et al., *MadDM v.3.0: a Comprehensive Tool for Dark Matter Studies*, *Phys. Dark Univ.* **24** (2019) 100249 [[1804.00044](#)].
7. G. Bélanger, F. Boudjema, A. Goudelis, A. Pukhov and B. Zaldivar, *micrOMEGAS 5.0 : Freeze-in*, *Comput. Phys. Commun.* **231** (2018) 173 [[1801.03509](#)].
8. N. D. Christensen, P. de Aquino, C. Degrande, C. Duhr, B. Fuks, M. Herquet et al., *A Comprehensive approach to new physics simulations*, *Eur. Phys. J. C* **71** (2011) 1541 [[0906.2474](#)].
9. E. Conte and B. Fuks, *Confronting new physics theories to LHC data with MADANALYSIS 5*, *Int. J. Mod. Phys. A* **33** (2018) 1830027 [[1808.00480](#)].
10. J. Y. Araz, M. Frank and B. Fuks, *Reinterpreting the results of the LHC with MadAnalysis 5: uncertainties and higher-luminosity estimates*, [1910.11418](#).
11. M. Backović, M. Krämer, F. Maltoni, A. Martini, K. Mawatari and M. Pellen, *Higher-order QCD predictions for dark matter production at the LHC in simplified models with  $s$ -channel mediators*, *Eur. Phys. J. C* **75** (2015) 482 [[1508.05327](#)].
12. D. Abercrombie et al., *Dark Matter Benchmark Models for Early LHC Run-2 Searches: Report of the ATLAS/CMS Dark Matter Forum*, *Phys. Dark Univ.* **26** (2019) 100371 [[1507.00966](#)].
13. C. Degrande, C. Duhr, B. Fuks, D. Grellscheid, O. Mattelaer and T. Reiter, *UFO - The Universal FeynRules Output*, *Comput. Phys. Commun.* **183** (2012) 1201 [[1108.2040](#)].
14. S. Frixione, B. Fuks, V. Hirschi, K. Mawatari, H.-S. Shao, P. A. Sunder et al., *Automated simulations beyond the Standard Model: supersymmetry*, *JHEP* **12** (2019) 008 [[1907.04898](#)].
15. J. Hisano, K. Ishiwata, N. Nagata and T. Takesako, *Direct Detection of Electroweak-Interacting Dark Matter*, *JHEP* **07** (2011) 005 [[1104.0228](#)].
16. Y. Bai and J. Berger, *Fermion Portal Dark Matter*, *JHEP* **11** (2013) 171 [[1308.0612](#)].
17. M. Garny, A. Ibarra, M. Pato and S. Vogl, *Internal bremsstrahlung signatures in light of direct dark matter searches*, *JCAP* **1312** (2013) 046 [[1306.6342](#)].



18. F. Giacchino, L. Lopez-Honorez and M. H. G. Tytgat, *Bremsstrahlung and Gamma Ray Lines in 3 Scenarios of Dark Matter Annihilation*, *JCAP* **1408** (2014) 046 [[1405.6921](#)].
19. M. Garny, A. Ibarra, S. Rydbeck and S. Vogl, *Majorana Dark Matter with a Coloured Mediator: Collider vs Direct and Indirect Searches*, *JHEP* **06** (2014) 169 [[1403.4634](#)].
20. M. Garny, A. Ibarra and S. Vogl, *Signatures of Majorana dark matter with  $t$ -channel mediators*, *Int. J. Mod. Phys. D* **24** (2015) 1530019 [[1503.01500](#)].
21. A. Ibarra and S. Wild, *Dirac dark matter with a charged mediator: a comprehensive one-loop analysis of the direct detection phenomenology*, *JCAP* **1505** (2015) 047 [[1503.03382](#)].
22. A. Berlin, D. S. Robertson, M. P. Solon and K. M. Zurek, *Bino variations: Effective field theory methods for dark matter direct detection*, *Phys. Rev. D* **93** (2016) 095008 [[1511.05964](#)].
23. J. Hisano, R. Nagai and N. Nagata, *Effective Theories for Dark Matter Nucleon Scattering*, *JHEP* **05** (2015) 037 [[1502.02244](#)].
24. P. Ko, A. Natale, M. Park and H. Yokoya, *Simplified DM models with the full SM gauge symmetry : the case of  $t$ -channel colored scalar mediators*, *JHEP* **01** (2017) 086 [[1605.07058](#)].
25. L. M. Carpenter, R. Colburn, J. Goodman and T. Linden, *Indirect Detection Constraints on  $s$  and  $t$  Channel Simplified Models of Dark Matter*, *Phys. Rev. D* **94** (2016) 055027 [[1606.04138](#)].
26. S. El Hedri, A. Kaminska, M. de Vries and J. Zurita, *Simplified Phenomenology for Colored Dark Sectors*, *JHEP* **04** (2017) 118 [[1703.00452](#)].
27. J. Hisano, R. Nagai and N. Nagata, *Singlet Dirac Fermion Dark Matter with Mediators at Loop*, *JHEP* **12** (2018) 059 [[1808.06301](#)].
28. S. Chang, R. Edezhath, J. Hutchinson and M. Luty, *Effective wimps*, *Physical Review D* **89** (2014) .
29. H. An, L.-T. Wang and H. Zhang, *Dark matter with- $t$ -channel mediator: A simple step beyond contact interaction*, *Physical Review D* **89** (2014) .
30. A. DiFranzo, K. I. Nagao, A. Rajaraman and T. M. Tait, *Simplified models for dark matter interacting with quarks*, *Journal of High Energy Physics* **2013** (2013) .
31. M. Papucci, A. Vichi and K. M. Zurek, *Monojet versus the rest of the world I:  $t$ -channel models*, *JHEP* **11** (2014) 024 [[1402.2285](#)].
32. K. A. Mohan, D. Sengupta, T. M. P. Tait, B. Yan and C. P. Yuan, *Direct Detection and LHC constraints on a  $t$ -Channel Simplified Model of Majorana Dark Matter at One Loop*, *JHEP* **07** (2019) 115 [[1903.05650](#)].
33. PARTICLE DATA GROUP collaboration, *Review of Particle Physics*, *Phys. Rev. D* **98** (2018) 030001.
34. P. Z. Skands et al., *SUSY Les Houches accord: Interfacing SUSY spectrum calculators, decay packages, and event generators*, *JHEP* **07** (2004) 036 [[hep-ph/0311123](#)].
35. C. Degrande, *Automatic evaluation of UV and R2 terms for beyond the Standard Model Lagrangians: a proof-of-principle*, *Comput. Phys. Commun.* **197** (2015) 239 [[1406.3030](#)].
36. T. Hahn, *Generating Feynman diagrams and amplitudes with FeynArts 3*, *Comput. Phys. Commun.* **140** (2001) 418 [[hep-ph/0012260](#)].
37. W. Hollik, J. M. Lindert and D. Pagani, *NLO corrections to squark-squark production and decay at the LHC*, *JHEP* **03** (2013) 139 [[1207.1071](#)].
38. S. Frixione, E. Laenen, P. Motylinski, B. R. Webber and C. D. White, *Single-top hadroproduction in association with a  $W$  boson*, *JHEP* **07** (2008) 029 [[0805.3067](#)].
39. NNPDF collaboration, *Parton distributions for the LHC Run II*, *JHEP* **04** (2015) 040 [[1410.8849](#)].
40. A. Buckley, J. Ferrando, S. Lloyd, K. Nordström, B. Page, M. Rüfenacht et al., *LHAPDF6: parton density access in the LHC precision era*, *Eur. Phys. J. C* **75** (2015) 132 [[1412.7420](#)].
41. P. Artoisenet, R. Frederix, O. Mattelaer and R. Rietkerk, *Automatic spin-entangled decays of heavy resonances in Monte Carlo simulations*, *JHEP* **03** (2013) 015 [[1212.3460](#)].
42. J. Alwall, C. Duhr, B. Fuks, O. Mattelaer, D. G. Öztürk and C.-H. Shen, *Computing decay rates for new physics theories with FeynRules and MadGraph5\_aMC@NLO*, *Comput. Phys. Commun.* **197** (2015) 312 [[1402.1178](#)].
43. T. Sjöstrand, S. Ask, J. R. Christiansen, R. Corke, N. Desai, P. Ilten et al., *An Introduction to PYTHIA 8.2*, *Comput. Phys. Commun.* **191** (2015) 159 [[1410.3012](#)].
44. S. Frixione and B. R. Webber, *Matching NLO QCD computations and parton shower simulations*, *JHEP* **06** (2002) 029 [[hep-ph/0204244](#)].
45. M. Cacciari, G. P. Salam and G. Soyez, *The anti- $k_t$  jet clustering algorithm*, *JHEP* **04** (2008) 063 [[0802.1189](#)].
46. M. Cacciari, G. P. Salam and G. Soyez, *FastJet User Manual*, *Eur. Phys. J. C* **72** (2012) 1896 [[1111.6097](#)].
47. E. Conte, B. Fuks and G. Serret, *MadAnalysis 5, A User-Friendly Framework for Collider Phenomenology*, *Comput. Phys. Commun.* **184** (2013) 222 [[1206.1599](#)].
48. R. Frederix, S. Frixione, F. Maltoni and T. Stelzer, *Automation of next-to-leading order computations in QCD: The FKS subtraction*, *JHEP* **10** (2009) 003 [[0908.4272](#)].
49. CMS collaboration, *Searches for physics beyond the standard model with the  $M_{T2}$  variable in hadronic final states with and without disappearing tracks in proton-proton collisions at  $\sqrt{s} = 13$  TeV*, **1909.03460**.
50. ATLAS collaboration, *Search for squarks and gluinos in final states with jets and missing transverse momentum using 139 fb $^{-1}$  of  $\sqrt{s} = 13$  TeV pp collision data with the ATLAS detector*, ATLAS-CONF-2019-040.
51. ATLAS collaboration, *Search for squarks and gluinos in final states with jets and missing transverse momentum using 36 fb $^{-1}$  of  $\sqrt{s} = 13$  TeV pp collision data with the ATLAS detector*, *Phys. Rev. D* **97** (2018) 112001 [[1712.02332](#)].
52. B. Fuks et al., *Proceedings of the first MadAnalysis 5 workshop on LHC recasting in Korea*, **1806.02537**.
53. D. Sengupta, *The MadAnalysis5 implementation of the ATLAS in monojet+missing energy*, 10.7484/INSPIREHEP.DATA.HUH5.239F.
54. ATLAS collaboration, *Search for dark matter and other new phenomena in events with an energetic jet and large missing transverse momentum using the ATLAS detector*, *JHEP* **01** (2018) 126 [[1711.03301](#)].
55. G. Chalons and H. Reyes-Gonzalez, *MadAnalysis 5 implementation of ATLAS-SUSY-16-07* (arXiv:1712.02332), 10.7484/INSPIREHEP.DATA.56DC.PPE2.
56. B. Dumont, B. Fuks, S. Kraml, S. Bein, G. Chalons, E. Conte et al., *Toward a public analysis database for LHC new physics searches using MADANALYSIS 5*, *Eur. Phys. J. C* **75** (2015) 56 [[1407.3278](#)].
57. DELPHES 3 collaboration, *DELPHES 3, A modular framework for fast simulation of a generic collider experiment*, *JHEP* **02** (2014) 057 [[1307.6346](#)].
58. A. L. Read, *Presentation of search results: The CL(s) technique*, *J. Phys. G* **28** (2002) 2693.
59. F. Giacchino, L. Lopez-Honorez and M. H. G. Tytgat, *Scalar Dark Matter Models with Significant Internal Bremsstrahlung*, *JCAP* **1310** (2013) 025 [[1307.6480](#)].



60. S. Colucci, B. Fuks, F. Giacchino, L. Lopez Honorez, M. H. G. Tytgat and J. Vandecasteele, *Top-philic Vector-Like Portal to Scalar Dark Matter*, *Phys. Rev. D* **D98** (2018) 035002 [[1804.05068](#)].
61. J. Edsjo and P. Gondolo, *Neutralino relic density including coannihilations*, *Phys. Rev. D* **D56** (1997) 1879 [[hep-ph/9704361](#)].
62. R. Iengo, *Sommerfeld enhancement: General results from field theory diagrams*, *JHEP* **05** (2009) 024 [[0902.0688](#)].
63. S. Cassel, *Sommerfeld factor for arbitrary partial wave processes*, *J. Phys. G* **G37** (2010) 105009 [[0903.5307](#)].
64. A. De Simone, G. F. Giudice and A. Strumia, *Benchmarks for Dark Matter Searches at the LHC*, *JHEP* **06** (2014) 081 [[1402.6287](#)].
65. F. Giacchino, A. Ibarra, L. Lopez Honorez, M. H. G. Tytgat and S. Wild, *Signatures from Scalar Dark Matter with a Vector-like Quark Mediator*, *JCAP* **1602** (2016) 002 [[1511.04452](#)].
66. A. Ibarra, A. Pierce, N. R. Shah and S. Vogl, *Anatomy of Coannihilation with a Scalar Top Partner*, *Phys. Rev. D* **D91** (2015) 095018 [[1501.03164](#)].
67. DES, FERMI-LAT collaboration, *Searching for Dark Matter Annihilation in Recently Discovered Milky Way Satellites with Fermi-LAT*, *Astrophys. J.* **834** (2017) 110 [[1611.03184](#)].
68. M. Drees and M. Nojiri, *Neutralino - nucleon scattering revisited*, *Phys. Rev. D* **D48** (1993) 3483 [[hep-ph/9307208](#)].
69. A. Djouadi and M. Drees, *QCD corrections to neutralino nucleon scattering*, *Phys. Lett. B* **B484** (2000) 183 [[hep-ph/0004205](#)].
70. J. Hisano, K. Ishiwata and N. Nagata, *Gluon contribution to the dark matter direct detection*, *Phys. Rev. D* **D82** (2010) 115007 [[1007.2601](#)].
71. P. Gondolo and S. Scopel, *On the sbottom resonance in dark matter scattering*, *JCAP* **1310** (2013) 032 [[1307.4481](#)].
72. V. Barger, W.-Y. Keung and D. Marfatia, *Bremsstrahlung in dark matter annihilation*, *Phys. Lett. B* **B707** (2012) 385 [[1111.4523](#)].
73. T. Toma, *Internal Bremsstrahlung Signature of Real Scalar Dark Matter and Consistency with Thermal Relic Density*, *Phys. Rev. Lett.* **111** (2013) 091301 [[1307.6181](#)].
74. S. Colucci, F. Giacchino, M. H. G. Tytgat and J. Vandecasteele, *Radiative corrections to vectorlike portal dark matter*, *Phys. Rev. D* **D98** (2018) 115029 [[1805.10173](#)].
75. A. Bouquet, P. Salati and J. Silk, *Gamma-Ray Lines as a Probe for a Cold Dark Matter Halo*, *Phys. Rev. D* **D40** (1989) 3168.
76. L. Bergstrom, *Radiative Processes in Dark Matter Photino Annihilation*, *Phys. Lett. B* **B225** (1989) 372.
77. S. Rudaz, *On the Annihilation of Heavy Neutral Fermion Pairs Into Monochromatic gamma-rays and Its Astrophysical Implications*, *Phys. Rev. D* **D39** (1989) 3549.
78. L. Bergstrom and P. Ullio, *Full one loop calculation of neutralino annihilation into two photons*, *Nucl. Phys. B* **B504** (1997) 27 [[hep-ph/9706232](#)].
79. Z. Bern, P. Gondolo and M. Perelstein, *Neutralino annihilation into two photons*, *Phys. Lett. B* **B411** (1997) 86 [[hep-ph/9706538](#)].
80. G. Bertone, C. B. Jackson, G. Shaughnessy, T. M. P. Tait and A. Vallinotto, *The WIMP Forest: Indirect Detection of a Chiral Square*, *Phys. Rev. D* **D80** (2009) 023512 [[0904.1442](#)].
81. FERMI-LAT collaboration, *Updated search for spectral lines from Galactic dark matter interactions with pass 8 data from the Fermi Large Area Telescope*, *Phys. Rev. D* **D91** (2015) 122002 [[1506.00013](#)].
82. H.E.S.S. collaboration, *Search for Photon-Linelike Signatures from Dark Matter Annihilations with H.E.S.S.*, *Phys. Rev. Lett.* **110** (2013) 041301 [[1301.1173](#)].
83. H.E.S.S. collaboration, *H.E.S.S. Limits on Linelike Dark Matter Signatures in the 100 GeV to 2 TeV Energy Range Close to the Galactic Center*, *Phys. Rev. Lett.* **117** (2016) 151302 [[1609.08091](#)].
84. M. Garny, J. Heisig, M. Hufnagel and B. Luelf, *Top-philic dark matter within and beyond the WIMP paradigm*, *Phys. Rev. D* **D97** (2018) 075002 [[1802.00814](#)].
85. PLANCK collaboration, *Planck 2018 results. VI. Cosmological parameters*, [1807.06209](#).
86. XENON collaboration, *Dark Matter Search Results from a One Ton-Year Exposure of XENON1T*, *Phys. Rev. Lett.* **121** (2018) 111302 [[1805.12562](#)].
87. PICO collaboration, *Dark Matter Search Results from the PICO-60 C<sub>3</sub>F<sub>8</sub> Bubble Chamber*, *Phys. Rev. Lett.* **118** (2017) 251301 [[1702.07666](#)].
88. J. Billard, L. Strigari and E. Figueroa-Feliciano, *Implication of neutrino backgrounds on the reach of next generation dark matter direct detection experiments*, *Phys. Rev. D* **D89** (2014) 023524 [[1307.5458](#)].
89. J. Einasto, *Dark Matter*, in *Astronomy and Astrophysics 2010*, [Eds. Oddbjorn Engvold, Rolf Stabell, Bozena Czerny, John Lattanzio], in *Encyclopedia of Life Support Systems (EOLSS)*, Developed under the Auspices of the UNESCO, Eolss Publishers, Oxford, UK, 2009, [0901.0632](#).
90. CTA CONSORTIUM collaboration, *Introducing the CTA concept*, *Astropart. Phys.* **43** (2013) 3.
91. A. Belyaev, N. D. Christensen and A. Pukhov, *CalcHEP 3.4 for collider physics within and beyond the Standard Model*, *Comput. Phys. Commun.* **184** (2013) 1729 [[1207.6082](#)].
92. J. M. Campbell and R. K. Ellis, *Update on vector boson pair production at hadron colliders*, *Physical Review D* **60** (1999) .
93. G. Belanger, F. Boudjema, A. Pukhov and A. Semenov, *micrOMEGAs4.1: two dark matter candidates*, *Comput. Phys. Commun.* **192** (2015) 322 [[1407.6129](#)].